FINAL REPORT

on

The Influence of Polarization on Millimeter Wave Propagation through Rain

C. W. BOSTIAN, W. L. STUTZMAN
PARIS H. WILEY and R. E. MARSHALL

Submitted To: National Aeronautics and Space Administration

Washington, D. C.

NASA GRANT NUMBER NGR-47-004-091

Covering the Period January 1, 1972, to December 31, 1973

January 1, 1974

Electrical Engineering Department

Virginia Polytechnic Institute and State University

Blacksburg, Virginia 24061

FINAL REPORT

ON

THE INFLUENCE OF POLARIZATION ON

MILLIMETER WAVE PROPATION THROUGH RAIN

C. W. BOSTIAN, W. L. STUTZMAN

PARIS H. WILEY AND R. E. MARSHALL

Submitted To: National Aeronautics and Space Administration

Washington, D. C.

NASA GRANT NUMBER NGR-47-004-091

Covering the Period January 1, 1972, to December 31, 1973

January 1, 1974

Electrical Engineering Department
Virginia Polytechnic Institute and State University
Blacksburg, Virginia 24061

TABLE OF CONTENTS

1. Introduction

1.1 Foreword

This report presents the essential findings of a twenty-seven month experimental and theoretical investigation into the influence of polarization on millimeter wave propagation through rain. The investigation was supported by NASA to explore (a) the limitations which precipitation depolarization will place on future millimeter wave earth-satellite communications systems employing orthogonal-polarization frequency sharing and (b) the possiblity of improving the fade resistance of such systems either through polarization diversity operation or by the choice of the polarization(s) least subject to attenuation. To facilitate the experimental work, the efforts described in this report were confined largely to ground-based communications systems. The theoretical results presented here will be extended more completely to satellite systems and 20 GHz satellite-to-ground propagation data will be collected in a subsequent VPI&SU project supported by NASA under Contract NAS5-21984.

1.2 Guide to Previous Reports

The three semi-annual status reports written for this project describe the experimental setup in detail and each volume presents accumulated data for the time period that it covers. These will be referenced in this document as Status Report I, etc.; and their full citations are as follows.

1. C. W. Bostian and W. L. Stutzman, "The Influence of Polarization on Millimeter Wave Propagation Through Rain," Semi-Annual Status Report I, NASA Grant NGR-47-004-091, VPI&SU, Blacksburg, July 1972 (NASA-CR-130107).

2. C. W. Bostian and W. L. Stutzman, "The Influence of Polarization on Millimeter Wave Propagation Through Rain," Semi-Annual Status Report II, NASA Grant NGR-47-004-091, VPI&SU, Blacksburg, January 1973 (NASA-CR-132074).

3. C. W. Bostian, W. L. Stutzman, P. H. Wiley, and R. E. Marshall, "The Influence of Polarization on Millimeter Wave Propagation Through Rain," Semi-Annual Status Report III, NASA Grant NGR-47-004-091, VPI&SU, Blacksburg, July 1973 (NASA-CR-132819).

One interim report (Interim Report I) was published in June, 1973, to present a new theoretical model for rain depolarization developed in the course of the project. A second interim report (Interim Report II) is now in preparation; it brings together all of the project data in one standard format. The full citations of the interim reports are:

1. P. H. Wiley, C. W. Bostian, and W. L. Stutzman, "The Influence of Polarization on Millimeter Wave Propagation Through Rain," Interim Report I, NASA Grant NGR-47-004-091, VPI&SU, Blacksburg, June 1973 (NASA-CR-132815).

2. C. W. Bostian, W. L. Stutzman, P. H. Wiley, and R. E. Marshall, "The Influence of Polarization on Millimeter Wave Propagation Through Rain," Interim Report II, NASA Grant NGR-47-004-091, VPI&SU, Blacksburg, April 1974.

In general, information contained in previous reports will be repeated here only when necessary for clarity.

1.3 Description of the Experiment

The experimental system used in this project is shown in Figure 1 (see Status Report I for complete details). Basically it consisted of a 1.43 km line-of-sight path with 4-foot (1.22 meter) diameter dual-polarized parabolic reflector antennas at each end. The antennas used were Control Data Corporation (TRG) question-mark mounted scalar feeds. Linearly polarized 17.65 GHz signals were transmitted with their electric field vectors at $+45^{o}$ and -45^{o} from the vertical. Initially these polarizations were chosen to maximize the measured depolarization at any given rainfall rate and thus provide as much data as possible. Later it was discovered that the cross polarization levels measured with $\pm 45^{o}$ linearly polarized signals are theoretically the least sensitive to variations in drop canting angle and this choice of polarizations greatly reduces the scatter in the data (in comparison, say, to that which is observed with horizontal and vertical polarization).

The antennas were designed for low residual (i.e. clear weather) cross polarization levels. When the system began operations on August 4, 1972, both channels indicated residual cross polarization isolations* of -51 dB. As the antennas aged and particularly after the transmitting antenna was invaded by a housefly (see Status Report II, page 3) this high degree of isolation could not be maintained on both channels. After

---

*Inverting P. A. Watson and M. Arbabi's (1973) definitions to match the data display conventions used in this report, cross polarization isolation is the decibel ratio of (a) the power coupled into one receiver channel from the orthogonally polarized transmitting antenna channel to (b) power coupled into the same receiver channel from the co-polarized transmitting antenna channel. See Chapter 3 for more details.

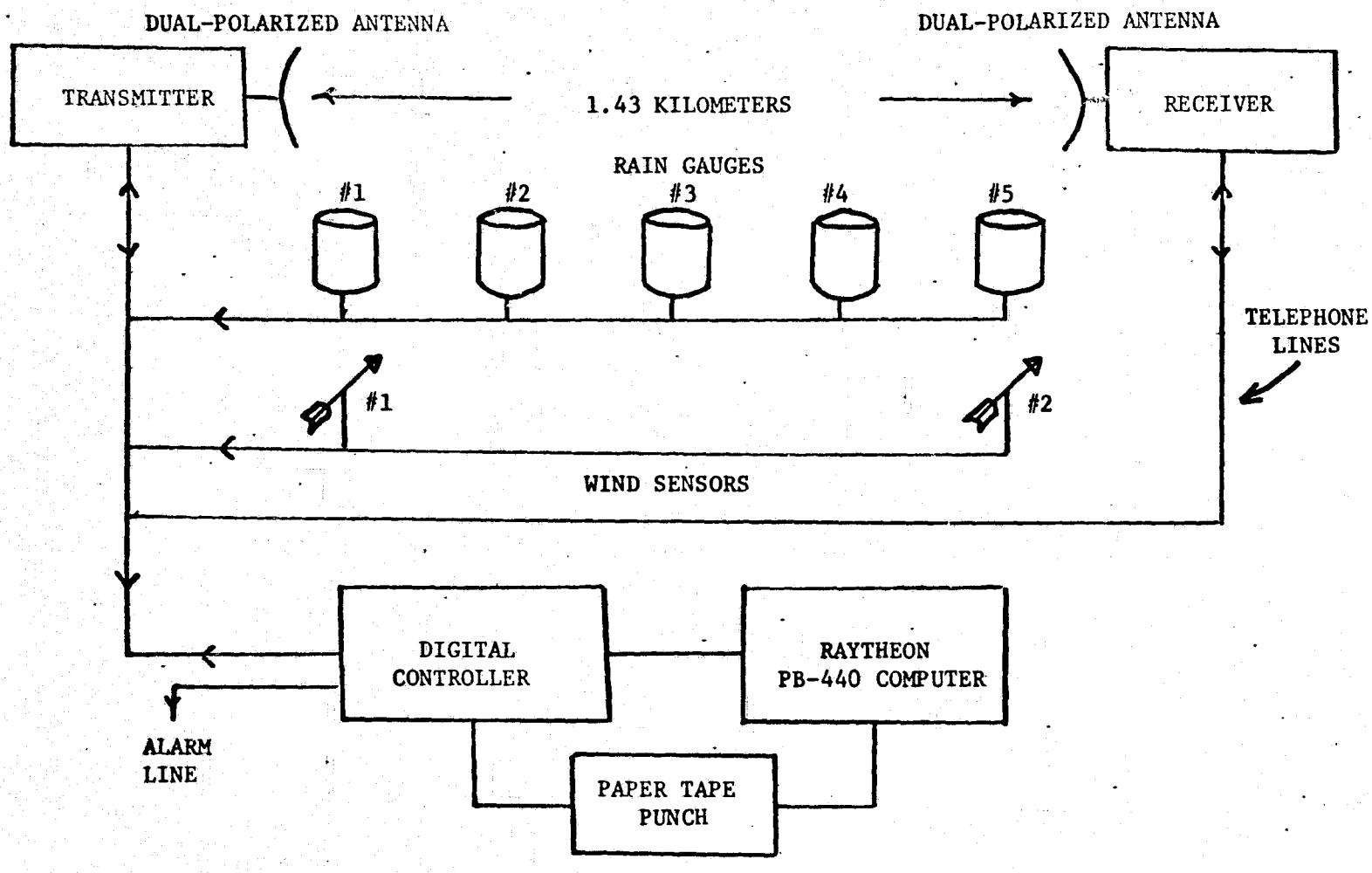

Figure 1. Experiment Block Diagram

October 6, 1972, the system operated with a nominal - to + isolation of -40 dB and a nominal + to - isolation of -20 dB. This inequality between the channels provided unexpected information on the way in which antenna characteristics influence observed values of rain depolarization.

The propagation path was carefully selected to eliminate depolarization by ground reflection or other multipath phenomenona. The common volume formed by the main beams of the two antennas did not intercept the ground or any other obstacle. The angle to the ground midpath from either antenna was 2^{o} and the angle from the mainbeam maximum to the first null of the radiation pattern was about 1^{o}. Therefore, only sidelobes intercepted the ground and any multipath effects were more than 40 dB below the direct signal.

Underneath the path were five tipping-bucket rain gauges, spaced about 300 meters apart. These were connected to the data processing system by leased telephone lines. Wind sensors were installed at two rain gauge locations.

A Raytheon PB 440 computer assisted by a special-purpose controller operated the experiment, acquired data, and performed preliminary data processing. The experimental control program maintained the system in the proper operating mode for existing weather conditions and signal behavior. The clear weather operating mode was called mode 0, and in it the $+45^{o}$ transmitter channel operated continuously while the computer monitored the $+45^{o}$ to -45^{o} cross polarization level and the $+45^{o}$ direct attenuation. Both receiver channels were sampled at 10 second intervals while wind velocity and transmitter power were sampled every 100 seconds. If the cross polarization level (in dB) changed by more than 2% or if

one of the rain gauges reported precipitation, the system began operating in mode 1. During mode 1 operation, transmission was sequenced at 4 second intervals from the $+45^{o}$ to the -45^{o} channel and then to both channels. Receiver sampling occurred at 1 second intervals and wind velocity was sampled every 4 seconds. Mode 1 operation continued until the precipitation rate fell below 6 mm/hr or until the cross polarization level stabilized. At this time, mode 2 operation began with transmitter switching at 10 second intervals and receiver and wind sampling at 2 and 10 second intervals respectively. Mode 2 operation continued until the precipitation rate fell below 3 mm/hr. The system then entered mode 3 with transmitter switching at 100 second intervals and receiver and wind sampling at 10 and 100 second intervals respectively. When the precipitation rate fell below 2 mm/hr, the system re-entered mode 0 operation. In all modes there was a low pass filter (time constant = 0.4 seconds) at the input to the A-D converter which surpressed fast scintillations of the signals and insured that average values were sampled.

When a new data point entered the PB 440 computer, a program located the last two values stored for the input. If the new value and the last value differed by more than 1%, the new value was stored. If the difference between the new value and the last value was less than 1%, the new value was compared to the next to last value. If these differed by more than 1%, the new value was stored; if this difference was less than 1%, the <u>last</u> value was discarded and the new value took its place.

An IBM 370/155 computer program was developed which processed, analyzed, and plotted the accumulated data from any number of selected storms. These data were rain rates from each gauge plus quasi-instantaneous (i.e. short integration time) samples of the analog signal levels during a storm. The latter were stored at essentially regular times while the intervals between successive rain gauge trips were random. Before data from different inputs could be compared, the computer was required to generate a time-function representation for each variable. These time functions were then averaged over selected time intervals to generate the average signal levels, rain rates, etc., required by steady state theory.

1.4 Data Collected

Rain data were collected and analyzed from August 4, 1972, through December 1, 1973. Tables 1.1 and 1.2 give the important parameters of each storm recorded. The data taken cover all but five of the intense rains which occurred; one 1972 storm and three 1973 storms were missed because of equipment failures, and at the time of writing the data from one 1973 storm is still out for copying from a 7-track magnetic tape to a 9-track magnetic tape.

During this project rain data were collected and analyzed for 24 individual storms in which the rain rate exceeded 10 mm/hr. These data represent 80408.6 seconds (22.34 hours) of rain, a net rain accumulation of 174.59 millimeters (6.87 inches), and 9940 recorded signal values.

Table 1. Summary of 1972 Storms

Date	Local Starting Time	Local Ending Time	Storm Duration, Seconds	Peak 15-second Averaged Path Rain Rate, mm/hr.	Total Rain Accumulation, mm					Number of Retained Data Points										
					RG #1	RG #2	RG #3	RG #4	RG #5	RG #1	RG #2	RG #3	RG #4	RG #5	R + T +	R + T -	R + T ±	R - T +	R - T -	R = T ±
Aug. 4	15:42:13.4	16:04:13.0	1319.6	37.3	3.81	-	-	-	3.05	15	-	-	-	12	68	110	90	-	-	-
Aug. 17	19:46:56.0	20:50:31.2	3815.2	104.2	6.35	-	-	-	9.10	25	-	-	-	36	15	28	21	20	18	18
Sept. 29	22:54:46.2	23:55:36.8	3650.6	45.5	4.57	-	4.32	4.32	4.57	18	-	17	17	18	44	116	62	58	41	37
Oct. 27	22:30:11.8	22:41:38.8	687.0	26.0	1.52	1.27	1.78	1.78	1.52	6	5	7	7	6	12	55	117	59	132	6
Nov. 13	22:20:54.8	23:03:43.0	2568.2	16.6	2.03	2.03	2.29	2.29	1.78	8	8	9	9	7	7	79	27	155	26	2
Nov. 14	00:20:13.4	00:55:34.6	2121.2	32.7	8.11	8.88	8.37	9.14	7.61	32	35	33	36	30	2	112	11	50	5	3

Table 2. Summary of 1973 Storms

Date	Local Starting Time	Local Ending Time	Storm Duration, Seconds	Peak 15-second Averaged Path Rain Rate, mm/hr	Total Rain Accumulation, mm					Number of Retained Data Points										
					RG #1	RG #2	RG #3	RG #4	RG #5	RG #1	RG #2	RG #3	RG #4	RG #5	T+ R+	T- R+	T± R+	T+ R-	T- R-	T± R-
March 16	16:26:34.4	19:57:08.4	12634.0	129.6	22.4	23.4	26.7	24.6	21.8	88	92	105	97	86	288	587	262	932	627	608
March 17	00:38:28.0	06:24:59.4	20791.4	35.7	7.4	15.5	13.2	16.0	14.5	29	61	52	63	57	105	239	69	939	65	47
May 23	21:26:31.6	21:38:46.2	734.6	41.7	3.6	4.6	*	3.0	2.8	14	18	0*	12	11	248	27	7	81	8	6
May 26	15:23:57.8	15:39:38.8	941.0	44.4	2.5	3.3	3.0	2.3	2.3	10	13	12	9	9	7	60	8	49	9	5
May 27	22:32:12.0	23:12:53.6	2441.6	48.3	6.9	7.1	5.8	6.9	5.3	27	28	23	27	21	11	63	7	100	6	5
May 28	01:03:34.0	02:19:16.2	4542.2	138.0	23.4	27.2	26.4	27.7	23.4	92	107	104	109	92	25	221	40	41	39	21

*Telephone company disconnected this gauge during line maintenance.

Table 2. Summary of 1973 Storms (Cont.)

Date	Local Starting Time	Local Ending Time	Storm Duration, Seconds	Peak 15-second Averaged Path Rain Rate, mm/hr	Total Rain Accumulation, mm					Number of Retained Data Points											
					RG #1	RG #2	RG #3	RG #4	RG #5	RG #1	RG #2	RG #3	RG #4	RG #5	+ T + R	- T + R	± T + R	+ T - R	- T - R	± T - R
ne 6	16:50:52.4	17:22:44.0	1911.6	49.5	4.1	4.6	4.3	4.8	3.3	16	18	17	19	13	19	23	19	77	13	11
ne 15	20:19:25.6	20:45:12.8	1547.2	36.3	5.3	6.1	0.0	8.1	4.8	21	24	0	32	19	12	43	54	80	32	5
ne 17	21:29:00.0	22:29:39.6	3639.6	91.2	34.8	33.3	0.0	36.6	27.9	137	131	0	144	110	12	31	17	92	22	13
ne 29	19:15:33.4	19:51:26.8	2153.4	42.7	3.0	3.6	0.0	3.8	3.3	12	14	0	15	13	35	45	47	88	25	12
ly 14	23:23:33.0	23:55:55/0	1942.0	55.6	13.5	13.5	14.2	14.5	11.9	53	53	56	57	47	39	90	65	124	34	7
ly 20	16:48:06.8	16:52:48.2	281.4	38.5	3.3	3.6	1.5	2.5	1.5	13	14	6	10	6	8	11	6	28	22	23
ly 22	13:10:34.4	13:18:22.8	468.4	63.8	5.3	5.3	2.5	3.8	3.6	21	21	10	15	14	48	20	28	31	5	5
gust 1	14:12:19.4	14:49:56.6	2257.2	68.6	0.0	7.9	15.2	18.0	14.5	0	31	60	71	57	59	91	80	71	29	23
gust 20	11:06:28.6	11:29:44.6	1396.0	53.1	3.6	4.8	0.0	7.9	9.1	14	19	0	31	36	14	18	30	45	23	10
tober 2	16:19:32.2	16:26:02.2	390.0	54.1	2.0	0.0	0.0	3.3	2.8	8	0	0	13	11	15	8	14	26	11	6

1.5 Acknowledgements

This report and the project it describes are the result of a dedicated effort by many individuals. The authors wish to thank the following for their contributions:

Mr. Erwin Hirschmann of NASA/GSFC for his continued assistance and encouragement.

Captain James L. Hogler, U.S. Army, for his many technical contributions.

Dr. A. Wayne Bennett and Mr. James A. Price of the VPI&SU EE Computer Engineering Laboratory for use of the PB 440 computer and associated equipment.

Dr. W. A. Blackwell, Dean W. J. Fabrycky, Dean P. E. Torgersen, and Vice President S. K. Cassell for continued administrative support of this project.

Mr. Harlow N. Pendrak for computer programming assistance.

Mrs. Sherida F. Battrell for typing this report and supervising its assembly.

2. The Theoretical Model

2.1 Introduction

When this project began the only theoretical means for predicting rain depolarization known to the authors was the differential attenuation model developed by Thomas [1971]. Since then, working independently, P. A. Watson's group at the University of Bradford (England) developed what we will call the propagation constant model [Watson and Arbabi, 1973], and the VPI&SU group derived the scattering model [Interim Report I]. A detailed derivation of the scattering model appeared in Interim Report I; this chapter expands the earlier development and shows how the scattering model relates to the propagation constant model.

2.2 The Scattering Model

The scattering model is based on summing up the scattered fields from each rain drop and evaluating them at the receiver location. The use of complex field representation allows calculation of attenuation, phase shift, and also cross polarization levels. The summing procedure turns out to be rather simple and allows for variation of many meteorological parameters. The details of the initial phases in the development of the scattering model can be found in the literature [Interim Report I; Wiley, Stutzman, and Bostian, 1973]. The model has been improved and can be used to make calculations, for instance, of rain scattering for long inhomogeneous paths. Also the accuracy of the model

has been closely examined. In this section the model improvements are discussed, tests of its accuracy are reported, and results of calculations are presented.

In Section 2.5, it will be shown that for homogeneous rains with all rain drops aligned the propagation constant or differential attenuation-differential phase shift model [Watson and Arbabi, 1973] is equivalent to the scattering model for large N (the number of path segments).

For convenient reference, the calculation procedure used with the scattering model is detailed in 2.6.1.

2.3 Improvements to the Scattering Model

In the initial phases of our theoretical research all calculations were made neglecting S_{21}, the term which accounts for scattering back into the main polarization from the generated cross polarized wave. This is a second order effect and does not become significant until the path length exceeds about 5 km. Thus all of our previously published theoretical curves based on the model (for a path length of 1 or 1.43 km) are very accurate. In order to make calculations for long paths, such as satellite-to-ground paths, the S_{21} term must be included. Note that we do not consider multiple scattering within a path segment, but we do include multiple scattering between segments. Let $E_1^{(i)}$ and $E_2^{(i)}$ be the main and cross polarized fields incident on the i^{th} segment. Then the main and cross polarized fields leaving that segment are given by

$$E_1^{(i+1)} = (1 + S_{11})\, E_1^{(i)} + S_{12} E_2^{(i)} \qquad (2\text{-}1)$$

$$E_2^{(i+1)} = S_{21}\, E_1^{(i)} + (1 + S_{22})\, E_2^{(i)} \tag{2-2}$$

where all fields are evaluated at the receiver location. Casting this into matrix notation we have

$$\begin{bmatrix} E_1^{(i+1)} \\ E_2^{(i+1)} \end{bmatrix} = \begin{bmatrix} 1 + S_{11} & S_{12} \\ S_{21} & 1 + S_{22} \end{bmatrix} \begin{bmatrix} E_1^{(i)} \\ E_2^{(i)} \end{bmatrix} \tag{2-3}$$

Denote the scattering matrix by $[S_{pq}]$. For N path segments we have for the first segment

$$\begin{bmatrix} E_1^{(i)} \\ E_2^{(i)} \end{bmatrix} = [S_{pq}] \begin{bmatrix} E_1^{(0)} \\ E_2^{(0)} \end{bmatrix} \tag{2-4}$$

For the second

$$\begin{bmatrix} E_1^{(2)} \\ E_2^{(2)} \end{bmatrix} = [S_{pq}] \begin{bmatrix} E_1^{(1)} \\ E_2^{(1)} \end{bmatrix} = ([S_{pq}])^2 \begin{bmatrix} E_1^{(0)} \\ E_2^{(0)} \end{bmatrix} \tag{2-5}$$

For the N^{th} segment

$$\begin{bmatrix} E_1^{(N)} \\ E_2^{(N)} \end{bmatrix} = ([S_{pq}])^N \begin{bmatrix} E_1^{(0)} \\ E_2^{(0)} \end{bmatrix} \tag{2-6}$$

and thus we have related the fields at the receiver with a free space propagation medium $E_1^{(0)}$ and $E_2^{(0)}$ to the fields propagating through the scattering medium $E_1^{(N)}$ and $E_2^{(N)}$ with due regard for polarization, amplitude, and phase. If the transmitting antenna is ideal $E_2^{(0)}$ will be zero; i.e.

there is no residual cross polarization. In this development we have assumed the scattering matrix to be identical for each segment. The scattering matrix for the entire path with N segments is

$$[S_{pq}^{(N)}] = ([S_{pq}])^N \tag{2-7}$$

This follows from the translocation theorem applied to homogeneous rains. Inhomogeneous rains may be easily accommodated by using different scattering matrices for different segments. For example, if the first half of the path is of uniform rain characteristics with scattering matrix $([S_{pq}])^{N/2}$ and the second half of the path is a uniform rain with characteristics different from the first half and denoted $([S'_{pq}])^{N/2}$ we have for the entire path a scattering matrix

$$[S_{pq}^{(N)}] = ([S'_{pq}])^{N/2} ([S_{pq}])^{N/2} \tag{2-8}$$

In general, these matrices are not commutative and, thus, order is important. In other words, a 100 mm/hr rain followed by a 50 mm/hr rain has different scattering properties than if the 50 mm/hr rain was followed by the 100 mm/hr rain; see Section 4.3.2.4 for an example of this effect.

If the main polarization is lined up along a principal axis of the rain ($\theta = 0^\circ$ or 90°), then S_{12} and S_{21} are zero and

$$[S_{pq}^{(N)}] = \begin{bmatrix} 1 + S_{11} & 0 \\ 0 & 1 + S_{22} \end{bmatrix}^N$$

$$= \begin{bmatrix} (1 + S_{11})^N & 0 \\ 0 & (1 + S_{22})^N \end{bmatrix} \tag{2-9}$$

for homogeneous rains.

Inclusion of the S_{21} term, of course, requires an expression for it. Its derivation parallels that of the Appendix in Interim Report I. If we find the corresponding single-drop scattering coefficient f_{21} we can find S_{21} (see 2.6.1). In Figure 2-1 an incident wave has its electric field vector along the 2 axis. The f_{21} coefficient is defined as

$$f_{21} = \frac{E_1^s}{E_2^i} \tag{2-10}$$

where E_2^i is the incident electric field intensity along the 2 axis and E_1^s is the forward scattered electric field intensity along the 1 axis, which is orthogonal to the 2 axis. E_2^i is decomposed into its principal axis components as follows:

$$E_{2v}^i = \sin\Theta\, E_2^i \tag{2-11}$$

$$E_{2h}^i = -\cos\Theta\, E_2^i \tag{2-12}$$

Note that we use v and h to denote the vertical and horizontal axes which are oriented along the minor and major axes of the drop. After passing through the drop the forward scattered field intensities along the drop principal axes are

$$E_{2v}^s = f_v\, E_{2v}^i \tag{2-13}$$

$$E_{2h}^s = f_h\, E_{2h}^i \tag{2-14}$$

where f_v and f_h are the single drop forward scattering coefficients along the principal axes. The scattered field which exists in the 1 direction

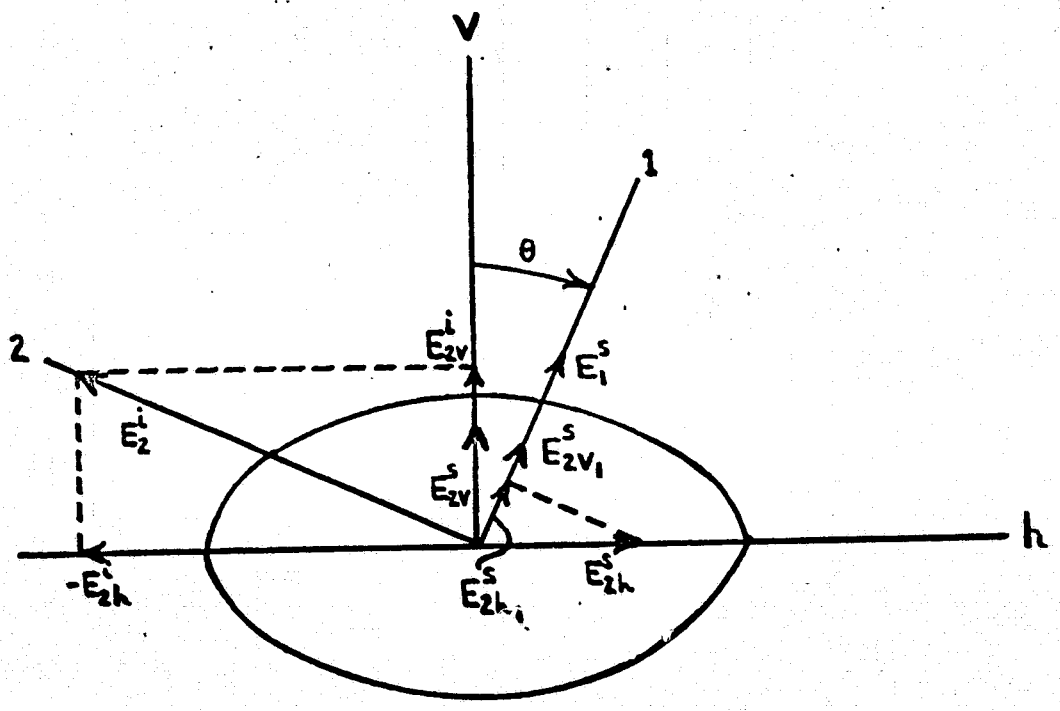

Figure 2-1 Single Drop Scattering Geometry for Computing f_{21}

is found from (see Figure 2-1)

$$E_1^s = E_{2v_1}^s + E_{2h_1}^s \tag{2-15}$$

But

$$E_{2v_1}^s = \cos\Theta\, E_{2v}^s \tag{2-16}$$

$$E_{2h_1}^s = \sin\Theta\, E_{2h}^s \tag{2-17}$$

Substituting these into (2-15) gives

$$E_1^s = \cos\Theta\, E_{2v}^s + \sin\Theta\, E_{2h}^s \tag{2-18}$$

Substituting (2-13) and (2-14) into (2-18) gives

$$E_1^s = f_v \cos\Theta\, E_{2v}^i + f_h \sin\Theta\, E_{2h}^i \tag{2-19}$$

Substituting (2-11) and (2-12) into (2-19) gives

$$E_1^s = (f_v - f_h) \sin\Theta \cos\Theta\, E_2^i \tag{2-20}$$

Using (2-20) in (2-10) gives the final result of

$$f_{21} = (f_v - f_h) \sin\Theta \cos\Theta \tag{2-21}$$

This is exactly the same expression that was found for f_{12} [Interim Report I], thus

$$f_{21} = f_{12} \tag{2-22}$$

Therefore, we also have (see 2.6.1)

$$S_{21} = S_{12} \tag{2-23}$$

The scattering model in all subsequent applications includes the S_{21} term.

2.4 Convergence of the Scattering Model

The calculated scattered field intensities at the receiver depend on N, the number of segments by which the path is divided. As one would expect, as N is increased the calculated values converge. However, N cannot be increased without limit. For N greater than about 50,000, values begin to fluctuate slightly - particularly phase values. A series of convergence tests were made to determine approximately what value of N should be used as a function of other parameters.

It turned out that convergence is not affected by Θ, the canting angle. The rain rate affects convergence somewhat. Most of the tests were run for a rain rate of 100 mm/hr. For rates less than this or greater than this, the convergence was slightly faster or slower, respectively. In all cases the phase (of the main and cross polarized signals) was the slowest to converge. The attenuation (or signal magnitudes) converged relatively fast. The cross polarization level converged very fast. The only remaining parameter is path length. In Table 2-1 suggested values of N are given for several path lengths. Also included in the table are estimated accuracies obtained when using these values of N. When using minicomputers to make these calculations, it may be necessary to use smaller values of N than those suggested.

Table 2-1 Suggested Values of N for Various Path Lengths

Path Length L, m	Number of Segments N	Estimated Accuracy		
		Cross Polarization Level, dB	Attenuation, dB	Phase, Degrees
1,000	5,000	0.01	0.01	0.1
2,500	5,000	0.01	0.02	0.2
5,000	5,000	0.01	0.05	0.3
7,500	10,000	0.01	0.1	0.5
10,000	10,000	0.01	0.1	1.0
15,000	15,000	0.01	0.3	2.0
20,000	20,000	0.01	0.5	2.0

If one is not interested in the phase, a value of N which is about 10% of that given will yield values which are accurate to within about 0.1 dB for cross polarization and 1 dB for attenuation. Due to round-off and error accumulation in computer calculations of this type, values of N which are far greater than those suggested are to be avoided.

2.5 Comparison with the Propagation Constant Model

In this section it is shown analytically and numerically that the scattering model and the propagation constant model [Watson and Arbabi, 1973] are nearly identical for certain situations, namely for a path along which the rain is homogenous and all drops are aligned. The propagation constant model is the only other existing model which can predict the attenuation, phase shift and cross polarization effects of an ensemble of raindrops. It is, however, limited to the case where all raindrops are aligned. A historical and theoretical review of the propagation constant model is found in Interim Report I .

In order to compare the two models we assume in this section a rain-filled path of uniform rain rate and we also assume that all drop principal axes are aligned.

2.5.1. Attenuation and Phase Shift along the Principal Axes of the Medium

If the incident electric field vector is along either the vertical axis or the horizontal axis the wave will propagate through the medium without polarization change. There will be, however, attenuation and phase shift relative to a free space propagation path of the same length. Since there is no depolarization f_{12} and f_{21} (and, thus, S_{12} and

and S_{21}) will be zero. This can be seen from (2-21) with $\Theta = 0^{\circ}$ (vertical) and $\Theta = 90^{\circ}$ (horizontal); in both cases f_{21} (and f_{12}) are zero. Let the 1 direction be the direction along which the E field is oriented, then the input fields are $E_1^{(0)} = 1$ and $E_2^{(0)} = 0$. From (2-9), the output scattered fields are $E_1^{(N)} = (1 + S_{11})^N$ and $E_2^{(N)} = 0$. But

$$S_{11} = - j \frac{4}{\pi} \frac{f_{11}}{L} N_D \tag{2-24}$$

where L is the path length in meters and N_D is the number of drops in a cell. Using (2-59) and $L = N\Delta\ell$ we have

$$N_D = nV \tag{2-25}$$

$$= n \frac{\pi\lambda\Delta\ell}{4} L[1 - \frac{\Delta\ell^2}{3L^2}]$$

$$= n \frac{\pi\lambda L}{4} \Delta\ell[1 - \frac{1}{3N^2}]$$

$$\simeq n \frac{\pi\lambda L}{4} \Delta\ell \qquad \text{for large N} \tag{2-26}$$

where n is the number of drops per cubic meter. Substituting (2-26) into (2-24) we have

$$S_{11} = - j\frac{4}{\pi} \frac{f_{11}}{N\Delta\ell} n \frac{\pi\lambda L}{4} \Delta\ell$$

$$S_{11} = - j \frac{n\lambda f_{11} L}{N} \qquad \text{for large N} \tag{2-27}$$

The result obtained by the propagation constant method is [van de Hulst, 1957]

$$e^{-jn\lambda f_{11}L} \tag{2-28}$$

which may be written as

$$e^{-jn\lambda f_{11}L} = \lim_{N\to\infty} \left(1 + \frac{-jn\lambda f_{11}L}{N}\right)^N \qquad (2\text{-}29)$$

Substituting (2-27) into $(1 + S_{11})^N$ gives

$$\left(1 + \frac{-jn\lambda f_{11}L}{N}\right)^N \qquad \text{for large N} \qquad (2\text{-}30)$$

We see that (2-30) is identical to (2-29) in the limit as N approaches infinity. Equation (2-30) was obtained from the scattering model and (2-29) from the propagation constant model. Thus, for large N the two models should be in close agreement.

If Θ is fixed at 0^o, the 1 direction is along the minor axis of the drop (vertical) and the 2 direction is along the major axis of the drop (horizontal). Then f_{11} and f_{22} are the vertical, f_v, and horizontal, f_h, single drop scattering coefficiants which are available from Oguchi [1973]. The propagation constant model computes the change in the received field intensity for a rain filled path of length L using propagation constants k_v and k_h for vertical and horizontal polarizations. The factor which gives the change in field intensity for vertical polarization is

$$e^{-jk_vL} \qquad \text{where } k_v = n\lambda f_v \qquad (2\text{-}31)$$

and for horizontal polarization is

$$e^{-jk_hL} \qquad \text{where } k_h = n\lambda f_h \qquad (2\text{-}32)$$

The scattering model gives $(1 + S_{11})^N$ and $(1 + S_{22})^N$ for the received vertical and horizontal fields. The comparison of these two models will

be carried out using a rain drop speed in m/sec of $4.6\sqrt{D_{mode}}$ and $D_{mode} = 1 + 0.9 \log (R)$ where D_{mode} is the mode drop diameter in mm and R is the rain rate in mm/hr [Interim Report I]. The results are independent of the percentage of oblate drops.

Table 2-2 compares the attenuations and phase shifts due to rains of several different rates for a 1 Km path in part (a) and for several path lengths at a rain rate of 100 mm/hr in part (b). Calculations for the scattering model were made using the values of N suggested by Table 2-1. Values for the two models agree extremely well in part (a). Differences between the attenuation and phase shift values obtained by the two models increase with increasing path length (see Table 2-2b). The differences are about the same as the estimated accuracy for attenuation and phase shift values given in Table 2-1. These differences are still quite small, especially considering that the example of 100 mm/hr rain over a 10 Km path is an extreme case. Note that the values in Table 2-2a are slightly different from those of Oguchi [1973] because of a different choice of raindrop speed and his use of a distribution of drop sizes.

2.5.2 Cross Polarization Calculations

In 2.5.1 it was shown that the attenuation and phase shift of a wave polarized along a principal axis of the medium (assuming that the principal axes of all raindrops are aligned) is calculated equally well by either the scattering model or the propagation constant model. We will now show that if the polarization of the transmitted signal is not along a principal axis, the attenuation, phase shift, and cross polarization predicted by both models are also the same.

Table 2-2 Comparison of the Scattering Model and the Propagation Constant Model for Attenuation and Phase Shift at 19.3 GHz

a) Path Length of 1 Km

	Attenuation (dB)				Phase (degrees)			
	Vertical Polarization		Horizontal Polarization		Vertical Polarization		Horizontal Polarization	
Rain Rate (mm/hr)	Scattering Model	Propagation Constant Model	Scattering Model	Propagation Constant Model	Scattering Model	Propagation Constant Model	Scattering Model	Propagation Constant Model
25.0	2.40	2.41	2.52	2.52	- 28.7	- 28.7	- 32.8	- 32.8
50.0	4.69	4.69	5.34	5.34	- 50.3	- 50.3	- 59.8	- 59.8
75.0	6.92	6.92	8.31	8.31	- 70.2	- 70.2	- 85.4	- 85.4
100.0	9.12	9.12	11.33	11.34	- 89.2	- 89.2	-110.0	-110.0
125.0	11.31	11.31	14.41	14.42	-107.6	-107.5	-133.9	-133.8
150.0	13.49	13.50	17.52	17.53	-125.4	-125.3	-157.1	-157.0

b) Rain Rate of 100 mm/hr

Path Length (Km)								
1.43	13.03	13.04	16.20	16.22	-127.5	-127.6	-157.2	-157.3
2.50	22.79	22.80	28.34	28.35	136.9	137.0	84.9	85.1
5.00	45.57	45.60	56.65	56.70	- 86.5	- 86.1	169.4	170.1
7.50	68.36	68.41	84.99	85.05	50.5	50.9	-105.5	-104.8
10.00	91.11	91.21	113.27	113.40	-172.7	-172.1	- 20.8	- 19.8

Consider a single rain cell of length L/N for which all drops are aligned. The coordinate system used is shown in Figure 2-1 for one drop. Note that we could just as easily frame this discussion around a single drop and use f coefficients instead of S coefficients. Let the transmit signal polarization be along the 1 direction. Then

$$E_1^t = E_{in}$$
$$E_2^t = 0 \tag{2-33}$$

The incident field can be decomposed into vertical and horizontal components as

$$E_v^t = E_{in} \cos \theta$$
$$E_h^t = E_{in} \sin \theta \tag{2-34}$$

After passing through one cell the received fields using the scattering model with vertical and horizontal axis decomposition is

$$\begin{bmatrix} E_v^r \\ E_h^r \end{bmatrix} = \begin{bmatrix} 1 + S_{vv} & 0 \\ 0 & 1 + S_{hh} \end{bmatrix} \begin{bmatrix} E_{in} \cos \theta \\ E_{in} \sin \theta \end{bmatrix} \tag{2-35}$$

which leads to

$$E_v^r = (1 + S_{vv})\, E_{in} \cos \theta \tag{2-36}$$

$$E_h^r = (1 + S_{hh})\, E_{in} \sin \theta \tag{2-37}$$

The scattering coefficients S_{vv} and S_{hh} are proportional to the single drop coefficients f_v and f_h (see 2.6.1). Let the proportionality constant be $C = -j4N_D/\pi L$. Then (2-36) and (2-37) become

$$E_v^r = E_{in} [\cos\theta + C f_v \cos\theta] \tag{2-38}$$

$$E_h^r = E_{in} [\sin\theta + C f_h \sin\theta] \tag{2-39}$$

If the scattering model is applied using the 1 and 2 axes for decomposition, the received fields are found from

$$\begin{bmatrix} E_1^r \\ E_2^r \end{bmatrix} = \begin{bmatrix} 1 + S_{11} & S_{12} \\ S_{21} & 1 + S_{22} \end{bmatrix} \begin{bmatrix} E_{in} \\ 0 \end{bmatrix} \tag{2-40}$$

which leads to

$$E_1^r = (1 + S_{11}) E_{in} \tag{2-41}$$

$$E_2^r = S_{21} E_{in} \tag{2-42}$$

To compare the received fields using these two decompostions the received fields along the vertical and horizontal axes of (2-41) and (2-42) are combined to form fields along the 1 and 2 axes. This is the logical way to make the comparison since the 1 and 2 directions are the main and cross polarized directions. The decomposition of E_v^r is

$$E^r_{v1} = \cos\theta\, E^r_v \qquad (2\text{-}43)$$

$$E^r_{v2} = \sin\theta\, E^r_v$$

and for E^r_h

$$E^r_{h1} = \sin\theta\, E^r_h \qquad (2\text{-}44)$$

$$E^r_{h2} = -\cos\theta\, E^r_h$$

The total field along the 1 direction after substitution of (2-36) and (2-37) into (2-43) and (2-44) is

$$E^r_{v1} + E^r_{h1} = E_{in}\,[\cos^2\theta\,(1 + S_{vv}) + \sin^2\theta\,(1+S_{hh})]$$

$$= E_{in}\,[1 + S_{vv}\cos^2\theta + S_{hh}\sin^2\theta] \qquad (2\text{-}45)$$

The total field along the 2 direction is

$$E^r_{v2} + E^r_{h2} = E_{in}\,[\sin\theta\cos\theta\,(1 + S_{vv}) - \sin\theta\cos\theta\,(1 + S_{hh})]$$

$$= E_{in}\sin\theta\cos\theta\,[S_{vv} - S_{hh}] \qquad (2\text{-}46)$$

Using (2-55) in (2-45) we have

$$E^r_{v1} + E_{h1} = E_{in}\,(1 + S_{11}) \qquad (2\text{-}47)$$

and using (2-55) with the percentage of oblate drops, P, equal to 100% in (2-46)

$$E^r_{v2} + E^r_{v2} = E_{in} S_{21} \qquad (2\text{-}48)$$

These are exactly the expressions of (2-41) and (2-42) which were obtained by using the 1 and 2 axes directly.

Thus, the change in the received fields due to rain can be calculated by the scattering model using axes along and perpendicular to the transmit polarization direction or using the principal axes of the medium. It was also shown previously that the change in the received fields along the principal axes computed by the scattering model was equivalent (in the limit) to the propagation constant method. Therefore, it is concluded that if the medium contains principal (or non-depolarizing) axes the change in the field intensity (amplitude, phase, and polarization) can be found by either the scattering model or the propagation constant model. For this to hold true the path must be filled with a homogeneous rain; in other words, the rain rate is uniform and all drops are alike, say 100% oblate.

The scattering model offers the advantages of easily accounting for a rain which is piecewise homogeneous. If the path is divided into N segements, each of these segments may have different rain rates, different percentages of drop shapes, and different canting angles. These features make the scattering model convenient to use for modeling real rains.

A numerical comparison of the scattering model and the propagation constant model will now be made to confirm the analytical derivations. We again assume an incident linearly polarized wave with its electric field vector at an angle θ with respect to the minor axis of oblate

drops which are all oriented the same way in a homogeneous rain. The ratio of the electric field in the cross polarized direction, 2, to the field in the main polarization direction, 1, at the receiver for one cell is found from (2-45) and (2-46) as

$$E^r_{v2} + E^r_{h2} = \frac{E_{in} \sin\theta \cos\theta [S_{vv} - S_{hh}]}{E_{in} [1 + S_{vv} \cos^2\theta + S_{hh} \sin^2\theta]}$$

$$= \frac{\sin\theta \cos\theta [S_{vv} - S_{hh}]}{(1 + S_{vv}) \cos^2\theta + (1 + S_{hh}) \sin^2\theta}$$

$$= \frac{\tan\theta [S_{vv} - S_{hh}]}{(1 + S_{vv}) + (1 + S_{hh}) \tan^2\theta} \qquad (2\text{-}49)$$

The propagation constant model results are obtained by letting $1 + S_{vv}$ be e^{-jk_vL} where $k_v = n\lambda f_v$ and $1 + S_{hh}$ be e^{-jk_hL} where $k_h = n\lambda f_h$. Then (2-49) becomes

$$\frac{\tan\theta [e^{-jk_vL} - e^{-jk_hL}]}{e^{-jk_vL} + e^{-jk_hL} \tan^2\theta} \qquad (2\text{-}50)$$

The cross polarization ratio in dB then follows as

$$XPOL_p = 20 \log \left| \frac{(1 - a) \tan\theta}{1 + a \tan^2\theta} \right| \qquad (2\text{-}51)$$

where

$$a = e^{-j(k_h - k_v)L} \qquad (2\text{-}52)$$

and the subscript p is used to denote propagation constant model. The expression in (2-50) is that obtained by Watson and Arbabi [1973]. Numerical results from this model will be compared to the scattering model as described in 2.6.1. The cross polarization ratio is compared in Table 2-3a for a 1 Km path and $\theta = 45^{o}$ as a function of rain rate. The percentage of oblate drops for Table 2-3 is 100%. In Table 2-3b the cross polarization ratio at a rain rate of 50 mm/hr is given as a function of path length for θ angles of 45^{o} and 60^{o}. Table 2-3c is the same as 2-3b except the rain rate is 100 mm/hr. The agreement in the cross polarization ratio between the two models is within a few hundredths of a dB for the wide range of parameters given in the table. These data confirm the analytical predictions.

2.6 Calculations Using the Scattering Model

2.6.1 Calculation Procedure

The fields at the receiver of a communication link with a free space propagation path are $E_1^{(0)}$ and $E_2^{(0)}$ where subscripts 1 and 2 refer to two orthogonal polarizations. The fields $E_1^{(N)}$ and $E_2^{(N)}$ are the fields at the receiver with a propagation medium along the link having N rain cells each of which is homogeneous. They are, in general, related by

$$\begin{bmatrix} E_1^{(N)} \\ E_2^{(N)} \end{bmatrix} = [S_{pq}^{(N)}]\,[S_{pq}^{(N-1)}] \cdots [S_{pq}^{(1)}] \begin{bmatrix} E_1^{(0)} \\ E_2^{(0)} \end{bmatrix} \qquad (2\text{-}53)$$

This allows for the possibility of modeling an inhomogeneous medium by one which is (longitudinally) cell-wise homogeneous. If the scattering

Table 2-3. Comparison of the Scattering Model and the Propagation Constant Model for Cross Polarization at 19.3 GHz

a) Cross polarization ratio in dB for a path length of 1. Km and $\Theta=45^{\circ}$

Rain Rate (mm/hr)	Scattering Model	Propagation Constant Model
12.5	-36.03	-36.03
25.0	-28.78	-28.78
50.0	-20.80	-20.80
75.0	-16.19	-16.19
100.0	-13.04	-13.04
125.0	-10.67	-10.67
150.0	- 8.80	- 8.80

b) Cross polarization ratio in dB for a rain rate of 50 mm/hr

	$\Theta = 45^{\circ}$		$\Theta = 60^{\circ}$	
Path Length (Km)	Scattering Model	Propagation Constant Model	Scattering Model	Propagation Constant Model
1.0	-20.80	-20.80	-21.89	-21.89
2.5	-12.76	-12.76	-13.62	-13.62
5.0	- 6.44	- 6.44	- 6.92	- 6.92
7.5	- 2.46	- 2.46	- 2.41	- 2.41
10.0	0.60	0.59	1.53	1.53
15.0	4.40	4.39	10.81	10.83
20.0	3.86	3.87	15.28	15.35

Table 2-3 (Cont.)

c) Cross polarization ratio in dB for a rain rate of 100 mm/hr

Path Length (Km)	$\Theta = 45^{\circ}$ Scattering Model	$\Theta = 45^{\circ}$ Propagation Constant Model	$\Theta = 60^{\circ}$ Scattering Model	$\Theta = 60^{\circ}$ Propagation Constant Model
1.0	-13.04	-13.04	-13.73	-13.74
2.5	- 4.87	- 4.88	- 4.62	- 4.63
5.0	1.10	1.08	4.49	4.47
7.5	2.35	2.34	10.00	9.97
10.0	1.20	1.20	7.28	7.28
15.0	- 0.25	- 0.25	4.26	4.27
20.0	- 0.06	- 0.06	4.67	4.65

properties of the cells are known the fields $E_1^{(N)}$ and $E_2^{(N)}$ are found by (2-53) for free space received fields $E_1^{(0)}$ and $E_2^{(0)}$. The attenuation, phase shift, and depolarization introduced by the scattering medium can then be calculated.

The scattering off of a single rain drop for vertical (minor axis) and horizontal (major axis) linear polarizations is known [Oguchi, 1973]. These single drop scattering coefficients for vertical and horizontal polarizations are the complex numbers f_v and f_h and they depend on the effective drop diameter. Oguchi used in his calculations a drop axial ratio of $1 - \frac{0.41}{9.00} D$ where D is the effective drop diameter. The single drop scattering coefficients for linear polarization 1 at an angle θ with respect to the drop minor axis polarization 2 orthogonal to 1 are [Interim Report I].

$$f_{11} = f_v \cos^2 \theta + f_h \sin^2 \theta$$

$$f_{12} = (f_v - f_h) \sin \theta \cos \theta \qquad (2\text{-}54)$$

$$f_{21} = f_{12}$$

$$f_{22} = f_v \sin^2 \theta + f_h \cos^2 \theta$$

The scattering coefficients for a cell containing N_D number of drops are

$$S_{11} = -j \frac{4}{L} f_{11} N_D = S_{vv} \cos^2 \theta + S_{hh} \sin^2 \theta$$

$$S_{12} = -j \frac{4}{\pi} \frac{f_{12}}{L} N_D P = (S_{vv} - S_{hh}) \sin \Theta \cos \Theta P \qquad (2\text{-}55)$$

$$S_{21} = S_{12}$$

$$S_{22} = -j \frac{4}{\pi} \frac{f_{22}}{L} N_D = S_{vv} \sin^2 \Theta + S_{hh} \cos^2 \Theta$$

where P is the percentage of oblate drops with scattering properties f_{11}, f_{12}, f_{21}, f_{22}. Note that Hogg [1973] introduced the percentage of oblate drops into the propagation constant model in an analogous fashion. To be strictly true a summation over a distribution of drops with different sizes and shapes should be used. This would require $f_{pq} N_D$ to be replaced by

$$\sum_{m=1}^{N_D} f_{pq}^{(m)} \qquad (2\text{-}56)$$

where $f_{pq}^{(m)}$ is the single drop scattering coefficient for the m^{th} drop. We have found this to be unnecessary. Instead the approximate relations (2-55) are used with the single drop scattering coefficients of the most frequently occurring drop with effective diameter D_{mode}. The mode drop diameter in mm is related to the rain rate R in mm/hr by

$$D_{mode} = 1 + 0.9 \log (R) \quad [mm] \qquad (2\text{-}57)$$

This is an empirical fit to Laws and Parsons data. The number of drops in a cell of width $\Delta\ell$ is

$$N_D = nV = 531 \frac{RV}{v_T D_{mode}^3} \tag{2-58}$$

where the volume of the cell is

$$V = \frac{\pi \lambda \Delta \ell}{4} \left[L - \frac{(\Delta \ell)^2}{3L} \right] \quad [m^3] \tag{2-59}$$

and the terminal velocity is [Best, 1950]

$$v_T = 4.6 \, D_{mode} \quad [m/sec] \tag{2-60}$$

The single drop scattering coefficients can be approximated as a polynomial function of the drop diameter by curve fitting to Oguchi's data. The results of this for 19.3 GHz are

$$\begin{aligned} f_v = [&0.0911 - j0.1939 + (-0.7043 + j1.8624) \frac{D_{mode}}{2} \\ &+ (1.7385 - j6.6664) \left(\frac{D_{mode}}{2}\right)^2 \\ &+ (-1.4076 + j11.7524) \left(\frac{D_{mode}}{2}\right)^3 \\ &+ (0.1045 - j11.31) \left(\frac{D_{mode}}{2}\right)^4 \\ &+ (0.6735 + j6.3222) \left(\frac{D_{mode}}{2}\right)^5 \\ &+ (-0.4549 - j2.0114) \left(\frac{D_{mode}}{2}\right)^6 \\ &+ (0.1165 + j0.3366) \left(\frac{D_{mode}}{2}\right)^7 \\ &+ (-0.0107 - j0.23) \left(\frac{D_{mode}}{2}\right)^8] \, 10^{-3} \end{aligned} \tag{2-61}$$

and

$$f_h = [0.2268 + j0.3191 + (-1.9326 - j2.8764)\frac{D_{mode}}{2}$$

$$+ (5.7933 + j9.6435)\left(\frac{D_{mode}}{2}\right)^2$$

$$+ (-7.8651 - j16.3873)\left(\frac{D_{mode}}{2}\right)^3$$

$$+ (5.5382 + j15.9783)\left(\frac{D_{mode}}{2}\right)^4$$

$$+ (-1.725 - j9.2378)\left(\frac{D_{mode}}{2}\right)^5$$

$$+ (0.0633 + j3.1876)\left(\frac{D_{mode}}{2}\right)^6$$

$$+ (0.0746 - j0.6041)\left(\frac{D_{mode}}{2}\right)^7$$

$$+ (-0.011 + j\ .048)\left(\frac{D_{mode}}{2}\right)^8] \ 10^{-3} \qquad (2\text{-}62)$$

All parameters have been given above for calculating the scattered fields at the receiver. From these we many calculate several quantities of interest for communication applications. Let $E_M^{(0)}$ be the field intensity at the receiver in the main polarization (transmit polarization) with no rain present. Frequently $E_2^{(0)}$ is set to zero and then $E_1^{(0)}$ equals $E_M^{(0)}$. The received signal in the main polarization after passing through a rain medium with N cells is denoted $E_M^{(N)}$. The field intensity at the receiver in the orthogonal polarization represents cross polarization and is denoted by $E_X^{(N)}$. If $E_2^{(0)} = 0$ then $E_M^{(N)} = E_1^{(N)}$ and $E_X^{(N)} = E_2^{(N)}$. The attenuation of the main signal is found from

$$A = 20 \log(|E_M^{(N)}|/|E_M^{(0)}|) \qquad [dB] \qquad (2\text{-}63)$$

The cross polarization level is defined by

$$XPOL = 20 \log(|E_X^{(N)}|/|E_M^{(N)}|) \qquad [dB] \qquad (2\text{-}64)$$

The additional phase shift introduced by the rain may also be of interest and is found from

$$PHASE_M = \text{Phase}\ (E_M^{(N)}) - \text{Phase}\ (E_M^{(0)}) \qquad (2\text{-}65)$$

$$PHASE_X = \text{Phase}\ (E_X^{(N)}) - \text{Phase}\ (E_X^{(0)}) \qquad (2\text{-}66)$$

where Phase ( ) is the operator which gives the phase angle of the complex argument.

As a final note, the scattering model as detailed here should not be used for rain rates less than one mm/hr. This is due to use of the mode drop diameter which is not a valid approach at very low rain rates. The scattering model gives good results at low rain rates if the distribution of drop sizes (for example, the Laws and Parsons distributions) is used. The effects of a distribution of drop sizes on cross polarization level are discussed by Hogler [1974] and summarized in Section 4.3.3.

2.6.2 Attenuation Calculations

The scattering model will be used to make calculations of attenuation for various rain rates, path lengths, and drop canting angles. In all cases the percentage of oblate drops, P, is 40%. This is an effective percentage obtained from the distribution of drop shapes in real rains. This value of P has led to good agreement between the model and our experiments; thus we will continue to use it here. The frequency used is 19.3 GHz.

In Figure 2-2 is plotted attenuation along 1 and 1.43 Km paths as a function of rain rate. For each path length there are curves for $\Theta = 0^{\circ}$ (vertical), 45°, and 90° (horizontal). Using the data presented by de Bettencourt [1973] one obtains an attenuation-rain rate relationship of $A = 0.105\ R^{1.017}$ dB/Km for R in mm/hr. This equation is empirical and was found from compiling data from many investigators and extrapolating. It agrees within a few tenths of a dB with the scattering model results for horizontal polarization. Since de Bettencourt makes no distinction between polarizations, little additional comparisons are possible.

In Figure 2-3 the attenuation is plotted versus path length for a rain rate of 50 mm/hr. These curves are linear. Thus, attenuations for other rain rates may be found from Figure 2-2. For example, the attenuation per Km from Figure 2-2 for a rain rate of 50 mm/hr and $\Theta = 0^{\circ}$ is 4.68 dB. Using this value for a 10 Km path leads to an attenuation of 46.8 dB. Figure 2- 3 shows a value of 46.8 dB also. Thus, the one kilometer attenuation values in Figure 2-2 can be used to find attenuations for other path lengths by linear extrapolation.

2.6.3 Phase Calculations

In this section we present the results of calculations with the scattering model at 19.3 GHz using 40% oblate drops. In Figures 2-4 and 2-5, the phase is plotted as a function of Θ for various rain rates for 1 and 1.43 Km paths. This phase is the phase change in the received signal with polarization angle Θ due to the rain. See (2-65). Notice that the phase changes rather slowly with Θ.

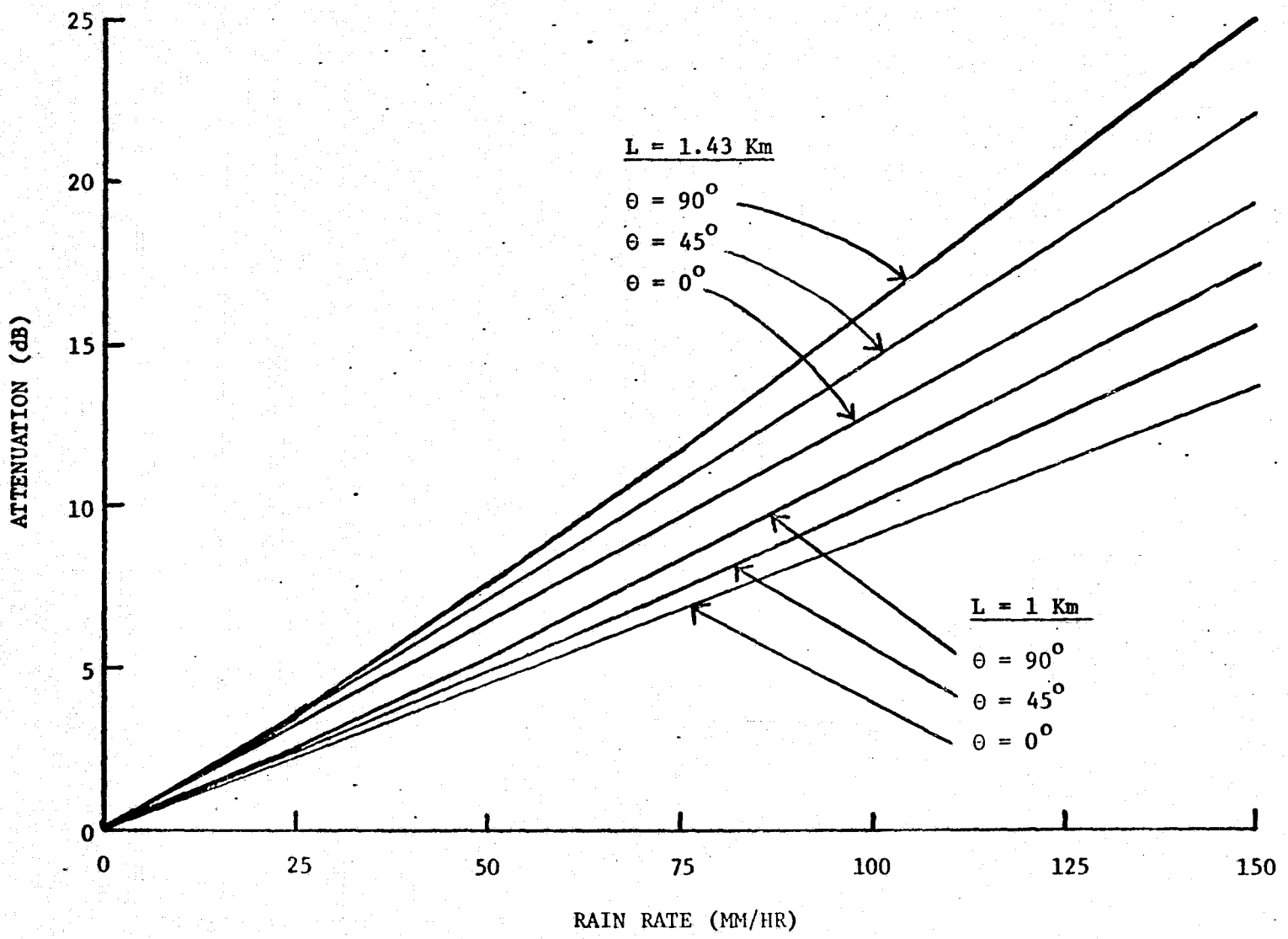

Figure 2-2 Attenuation versus rain rate: calculated from the scattering model using 40% oblate drops and a frequency of 19.3 GHz.

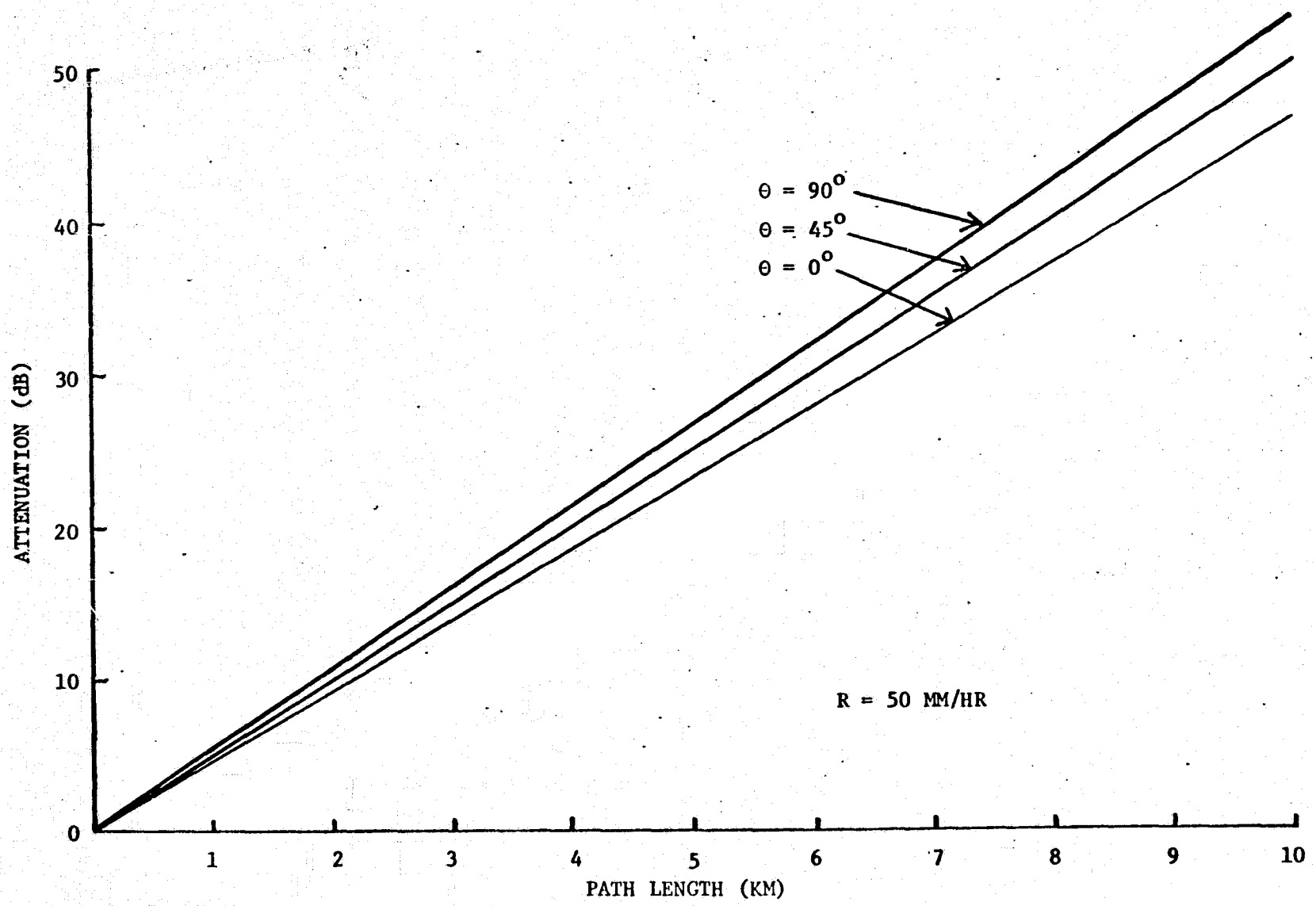

Figure 2-3 Attenuation versus path length for a rain rate of 50 mm/hr: calculated from the scattering model using 40% oblate drops and a frequency of 19.3 GHz.

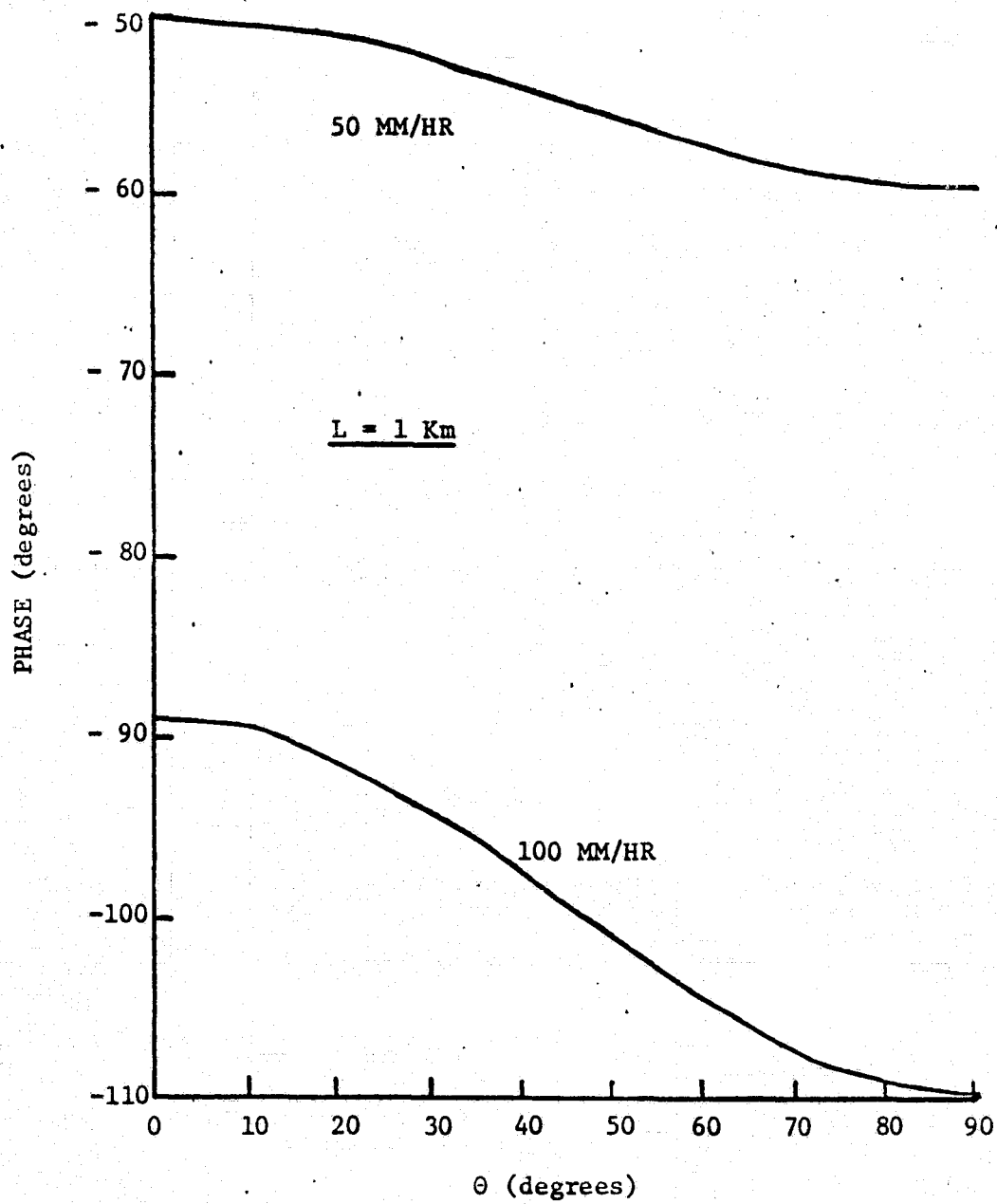

Figure 2-4 Phase shift of a wave with polarization angle Θ due to introduction of rain over the 1 Km path at 19.3 GHz.

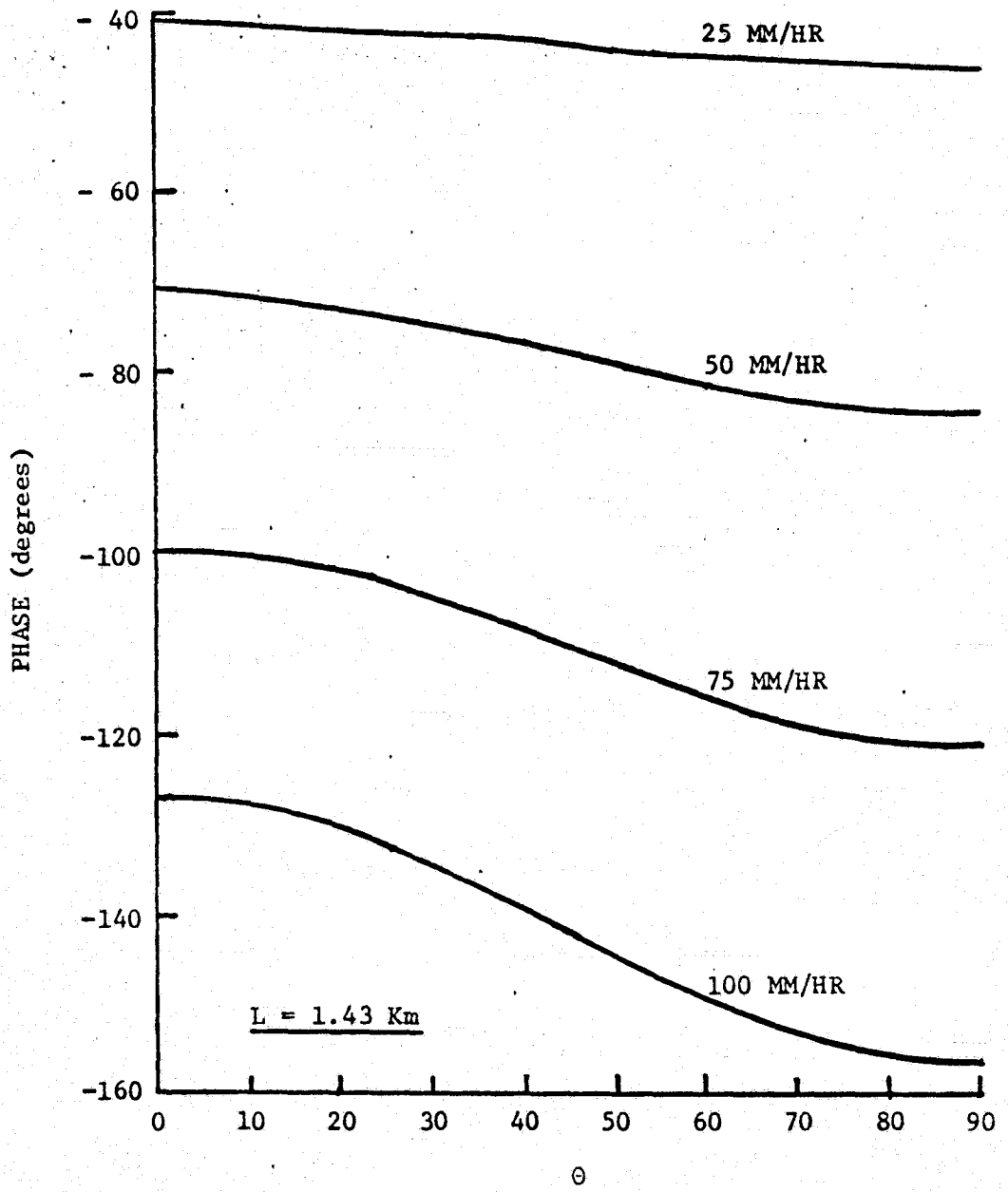

Figure 2-5 Phase shift of a wave with polarization angle Θ due to introduction of rain over the 1.43 Km path at 19.3 GHz.

2.6.4 Cross Polarization Calculations

The scattering model can be used to calculate cross polarization level as given in (2-64). In this section the cross polarization levels for various rain rates, path lengths, and canting angles are presented. The percentage of oblate drops is 40% and the frequency is 19.3 GHz.

In Figure 2-6 the cross polarization level is plotted versus rain rate for a 1 Km path and a polarization angle of 45°. In Figure 2-7 the cross polarization level is plotted for various rain rates as a function of path length for $\Theta = 45^{\circ}$. These curves are nonlinear. Therefore, extrapolation from the 1 Km values is not possible and several plots are required to show how cross polarization depends on the parameters. As shown previously attenuation and phase shift are not strongly dependent on Θ; however, the cross polarization level does depend greatly on Θ. Figure 2-8 shows this dependence for a 50 mm/hr rain. Of course, the depolarization vanishes along the principal axes ($\Theta = 0^{\circ}$ and 90°). In Figure 2-9 the dependence on Θ is plotted for a 100 mm/hr rain and various path lengths. In extreme situations (long paths and high rain rates) the cross polarization level can actually go positive. This means that the cross polarized field is stronger than the field intensity in the main polarization. [This is, of course, also found to be true using the propagation constant model (see Table 2-3).] It occurs because of the different phase shifts encountered. Note that the cross polatization level is <u>not</u> symmetric about $\Theta = 45^{\circ}$. The asymmetry becomes more pronounced for extreme situations.

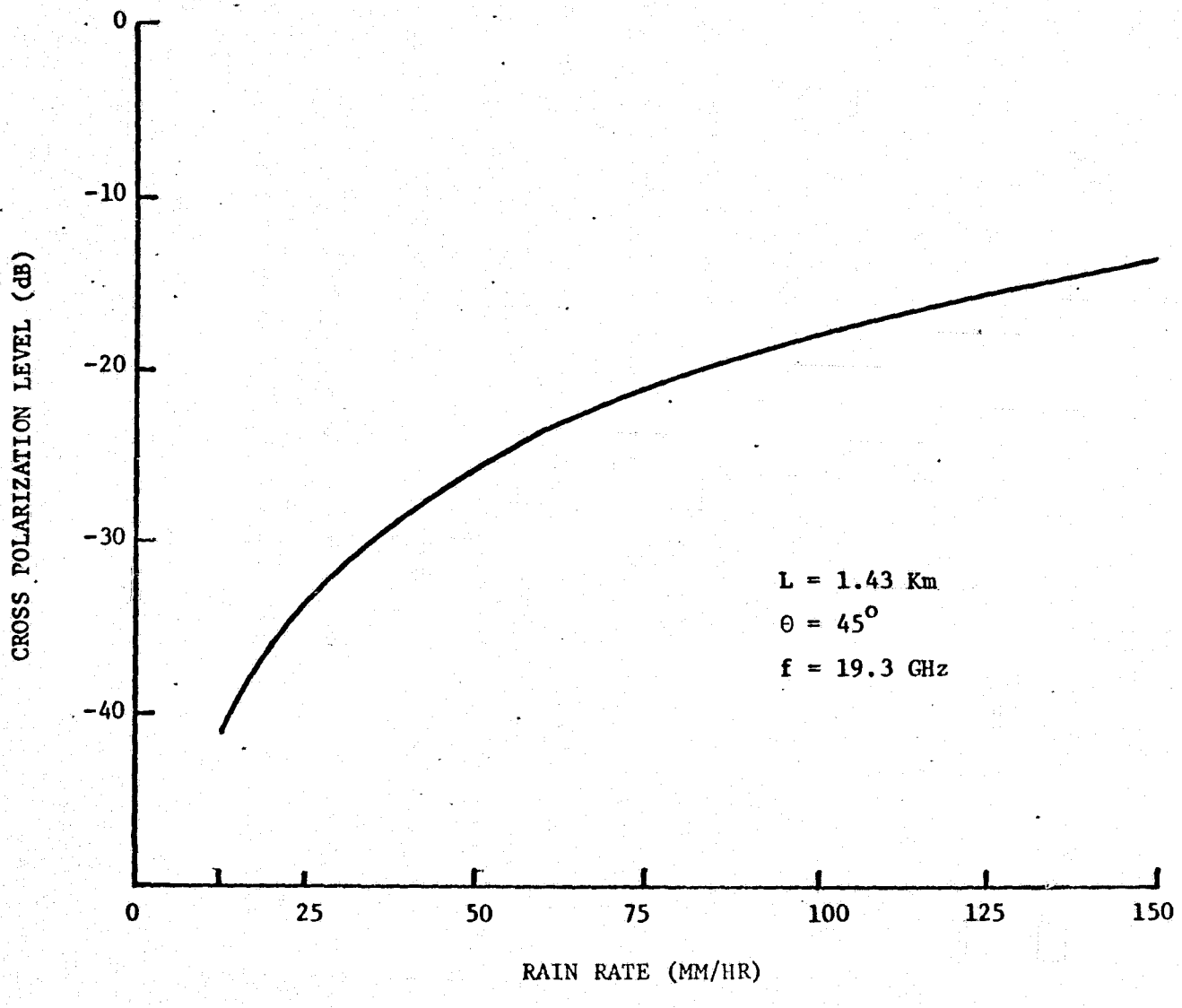

Figure 2-6 Cross polarization level versus rain rate: calculated from the scattering model for $\theta = 45^{\circ}$, a path length of 1.43 Km, and 19.3 GHz.

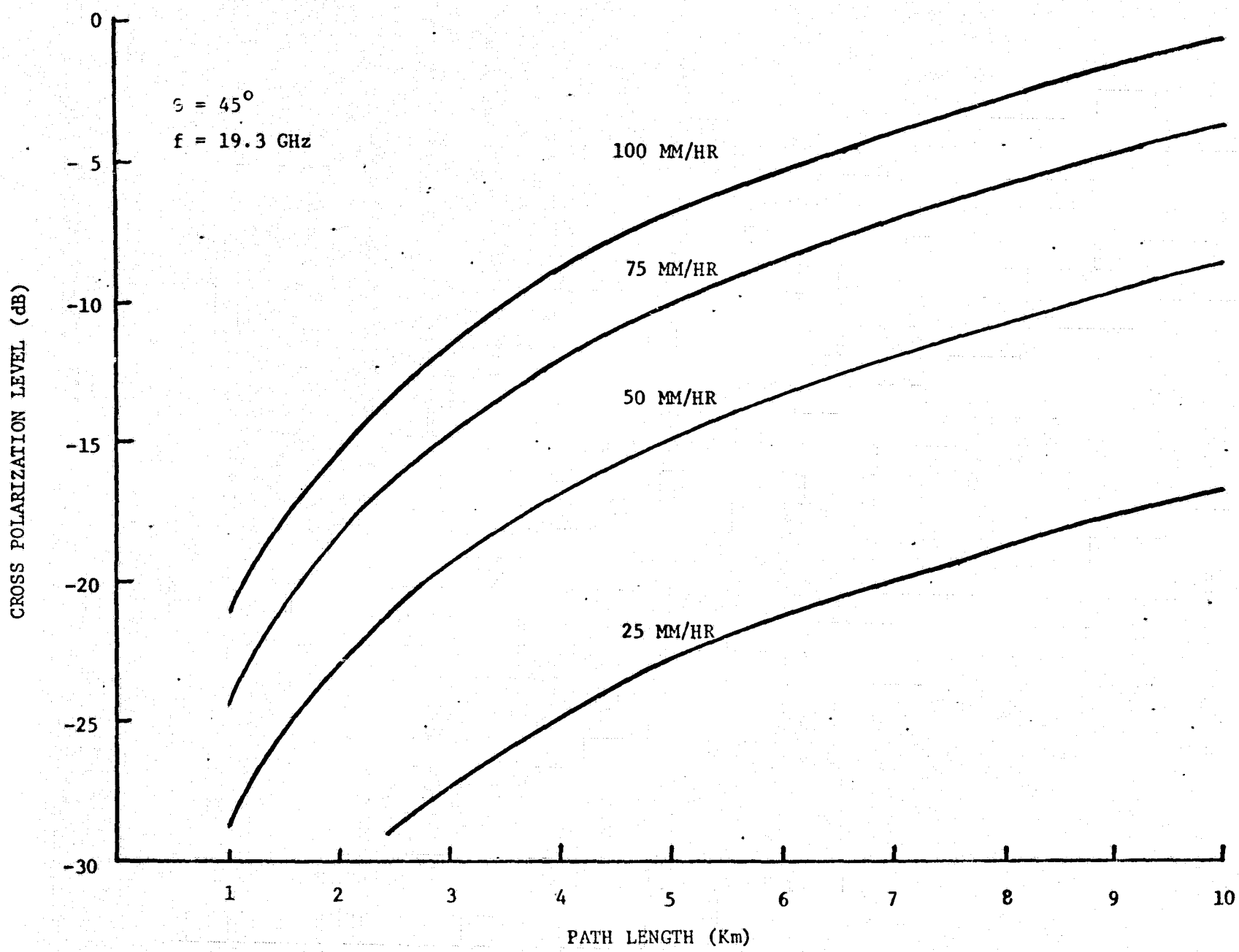

Figure 2-7 Cross polarization level versus path length: calculated from the scattering model for $\theta = 45^{\circ}$ and 19.3 GHz.

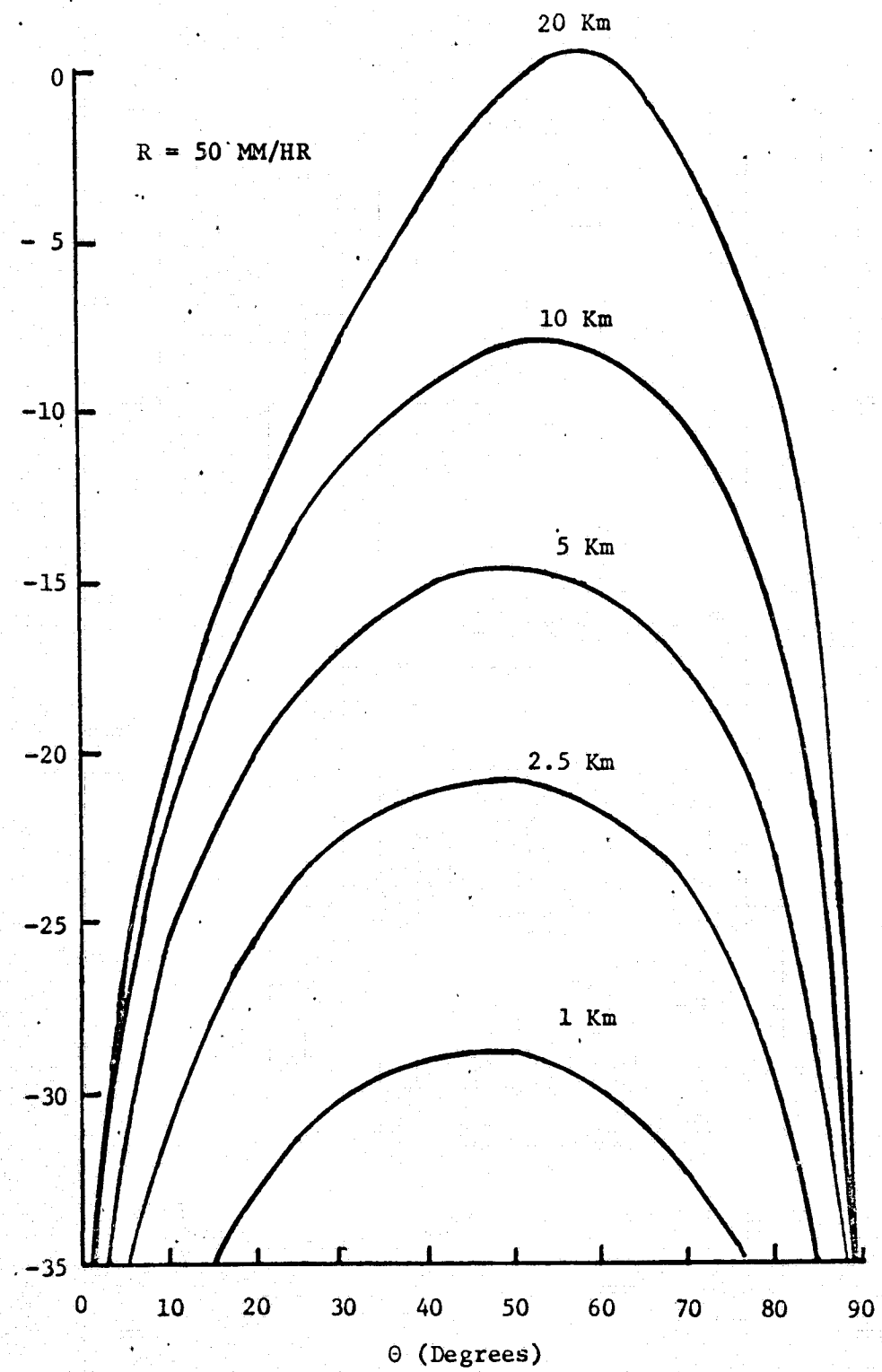

Figure 2-8 Cross polarization level versus Θ: calculated from the scattering model for a 50 mm/hr rain at 19.3 GHz.

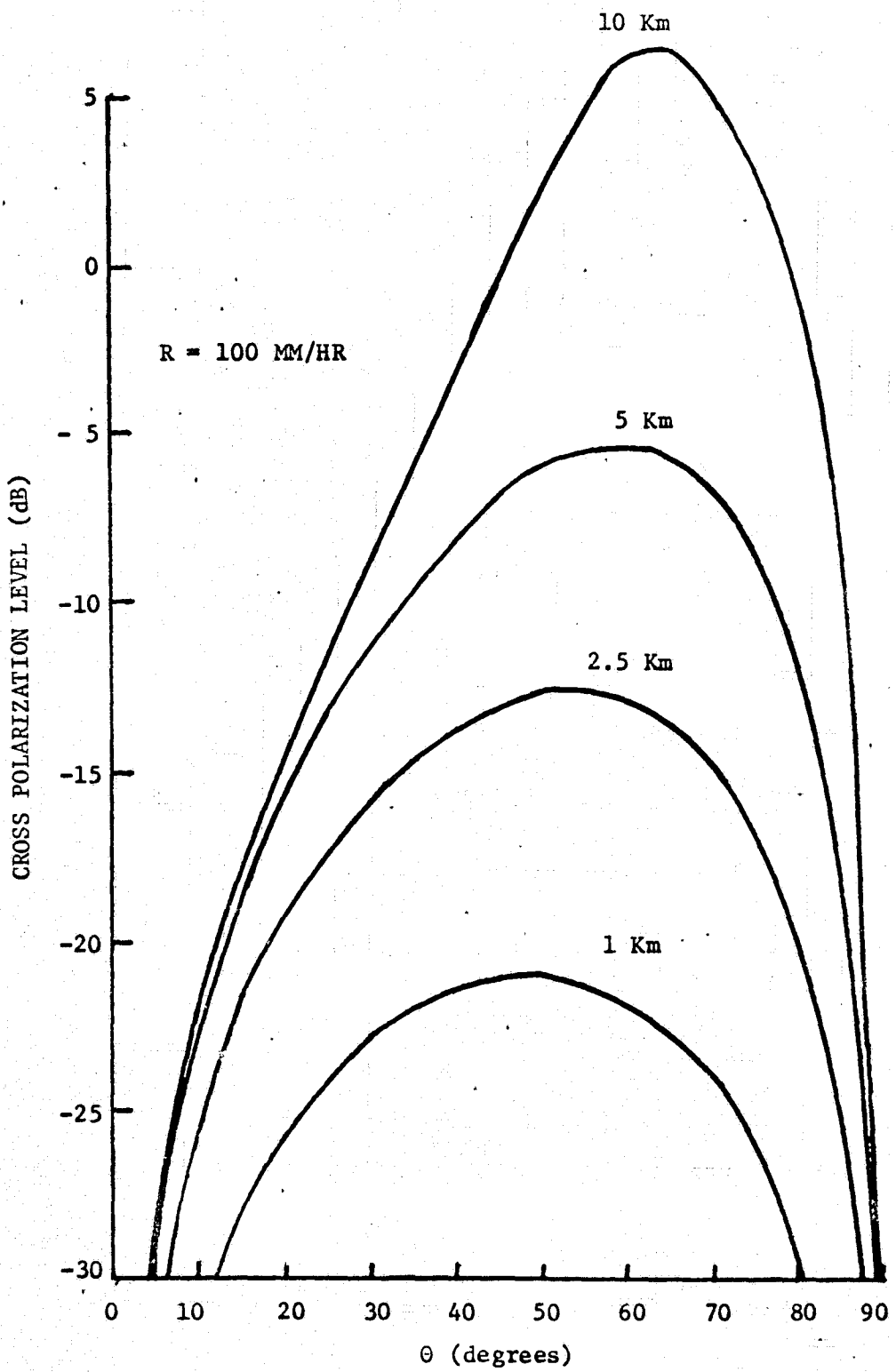

Figure 2-9 Cross polarization level versus Θ: calculated from the scattering model for a 100 mm/hr rain at 19.3 GHz.

In Figure 2-10 the cross polarization level is plotted for a 1.43 Km path as a function of θ for several rain rates.

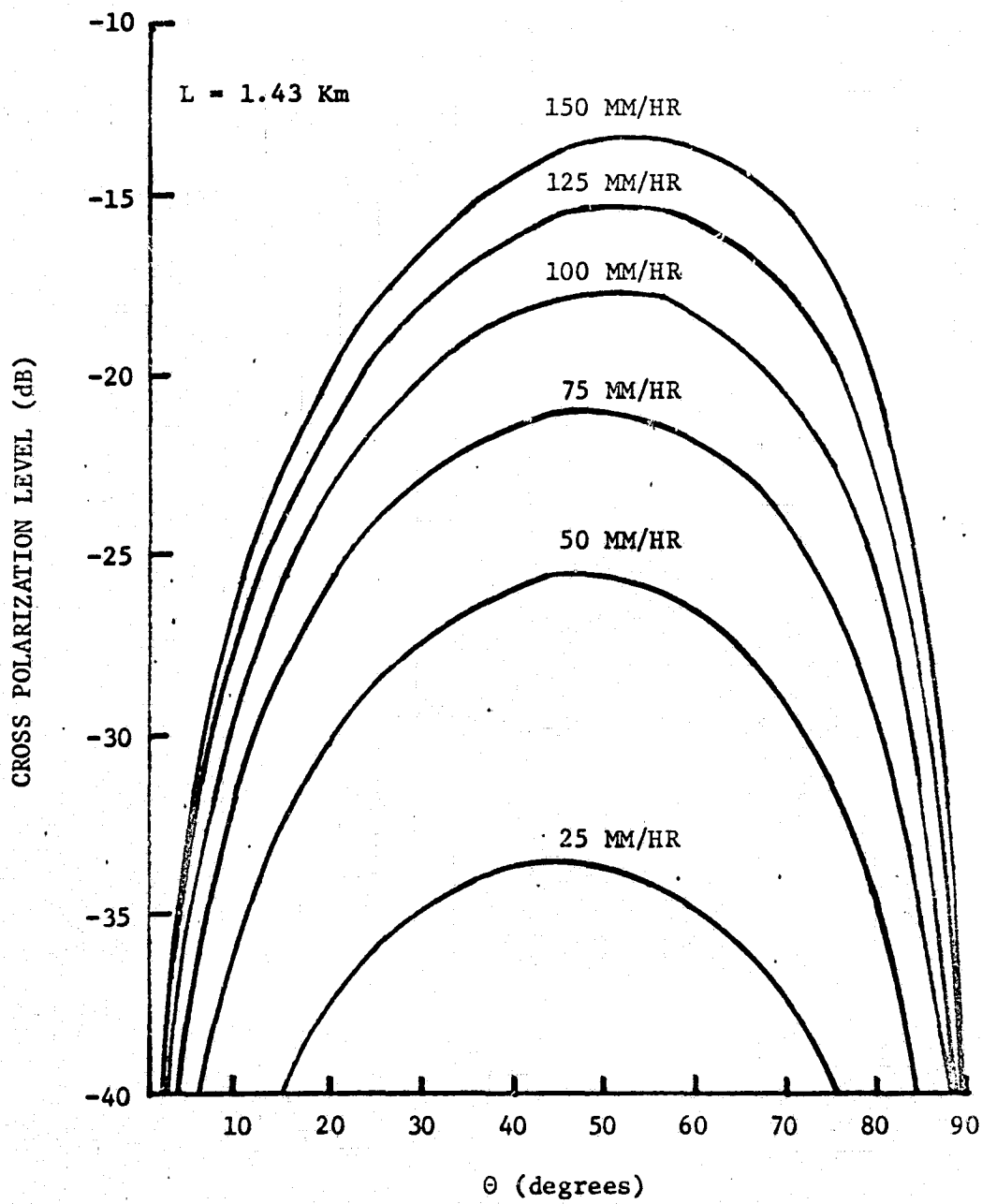

Figure 2-10 Cross polarization level versus Θ: calculated from the scattering model for a 1.43 Km path at 19.3 GHz.

3. Cross Polarization Effects in a Complete Communications Systems

3.1 Introduction

The cross polarization levels measured in any communications system using non-ideal components are a complicated function of the transmitting antenna, receiving antenna, and propagation path characteristics To provide suitable background for the data discussion which follows in the next chapter, this chapter examines some of the relationships that are involved.

3.2 Representing a Communications System

3.2.1 The Mathematical Model

Visualize a communications system employing two orthogonal polarizations identified by the numbers 1 and 2. The transmitting and receiving antennas each have two feeds, one coupling primarily (but not exclusively) to each polarization. Let each feed be connected to a matched transmission line and define a set of normalized voltages V_1^T, V_2^T, V_1^R, and V_2^R such that

$$P_1^T = V_1^T V_1^{T*} \tag{3-1}$$

is the input power to feed 1 on the transmitting antenna,

$$P_1^R = V_1^R V_1^{R*} \tag{3-2}$$

is the power delivered by feed 1 on the receiving antenna to a matched load, etc. The complete system can be visualized as an equivalent four-port network with inputs V_1^T and V_2^T and outputs V_1^R and V_2^R. The overall network transfer function can be broken down into the product of three matrices: one for the transmitting antenna, one for the path, and one for the receiving antenna.

The antennas can be represented as transducers between a set of normalized transmission line voltages and a set of orthogonal E field components in space. Choose a pair of coordinate axes mutually orthogonal to each other and to the direction of propagation and let far-field complex phasor components along these axes of the E field at the transmitting antenna aperture be E_1^T and E_2^T. The transfer function of the transmitting antenna can be defined by

$$\begin{bmatrix} E_1^T \\ E_2^T \end{bmatrix} = \begin{bmatrix} S_{11}^T & S_{12}^T \\ S_{21}^T & S_{22}^T \end{bmatrix} \begin{bmatrix} V_1^T \\ V_2^T \end{bmatrix} \tag{3-3}$$

Similarly the receiving antenna couples the E field at its aperture to V_1^R and V_2^R. If E_1^R and E_2^R are the phasor spatial components of the receiving antenna aperture E field, then the transfer behavior of the antenna is defined by

$$\begin{bmatrix} V_1^R \\ V_2^R \end{bmatrix} = \begin{bmatrix} S_{11}^R & S_{12}^R \\ S_{21}^R & S_{22}^R \end{bmatrix} \begin{bmatrix} E_1^R \\ E_2^R \end{bmatrix} \tag{3-4}$$

The propagation path also behaves as a four-port network connecting E_1^T and E_2^T to E_1^R and E_2^R. The relationship is

$$\begin{bmatrix} E_1^R \\ E_2^R \end{bmatrix} = \begin{bmatrix} S_{11}^P & S_{12}^P \\ S_{21}^P & S_{22}^P \end{bmatrix} \begin{bmatrix} E_1^T \\ E_2^T \end{bmatrix} \tag{3-5}$$

The path matrix elements S_{11}^P, S_{12}^P, S_{21}^P, and S_{22}^P may be calculated from the scattering model. In the notation of equation (2-53),

$$S_{11}^P = \left. \frac{E_1^{(N)}}{E_1^{(0)}} \right|_{E_2^{(0)} = 0} \tag{3-6}$$

$$S_{12}^P = \left. \frac{E_1^{(N)}}{E_2^{(0)}} \right|_{E_1^{(0)} = 0} \tag{3-7}$$

$$S_{21}^P = \left. \frac{E_2^{(N)}}{E_1^{(0)}} \right|_{E_2^{(0)} = 0} \tag{3-8}$$

$$S_{22}^P = \left. \frac{E_2^{(N)}}{E_2^{(0)}} \right|_{E_1^{(0)} = 0} \tag{3-9}$$

The transfer equation for the complete system is found by combining (3-3), (3-4), and (3-5).

$$\begin{bmatrix} V_1^R \\ V_2^R \end{bmatrix} = \begin{bmatrix} S_{11}^R & S_{12}^R \\ S_{21}^R & S_{22}^R \end{bmatrix} \begin{bmatrix} S_{11}^P & S_{12}^P \\ S_{21}^P & S_{22}^P \end{bmatrix} \begin{bmatrix} S_{11}^T & S_{12}^T \\ S_{21}^T & S_{22}^T \end{bmatrix} \begin{bmatrix} V_1^T \\ V_2^T \end{bmatrix} \quad (3\text{-}10)$$

3.2.2 Calculating the Matrix Elements

3.2.2.1 Receiving Antennas. Like many matrix equations, (3-10) is easier to write down than to use! The elements of the path matrix are available from any of the techniques for analyzing rain scatter but conventional antenna data do not usually provide enough information to fill in the antenna matrices. The additional data needed can be developed by measurement or from the normalized Stokes parameters [Kraus and Carver, 1973].

For the Stokes approach let the normalized Stokes parameters of the receiving antenna be (a_o,a_1,a_2,a_3) for feed 1 and (b_o,b_1,b_2,b_3) for feed 2. Let the corresponding effective apertures be Ae_1 and Ae_2. In terms of E_1^R and E_2^R, the normalized Stokes parameters of the incident wave are

$$s_o = 1 \quad (3\text{-}11)$$

$$s_1 = \frac{|E_1^R|^2 - |E_2^R|^2}{|E_1^R|^2 + |E_1^R|^2} \quad (3\text{-}12)$$

$$s_2 = \frac{2|E_1^R||E_2^R| \cos \delta}{|E_1^R|^2 + |E_2^R|^2} \quad (3\text{-}13)$$

$$s_3 = \frac{2|E_1^R||E_2^R| \sin \delta}{|E_1^R|^2 + |E_2^R|^2} \tag{3-14}$$

The phase angle between E_1^R and E_2^R is δ.

The Poynting vector amplitude of the incident wave may be written as

$$S = \frac{|E_1^R|^2 + |E_2^R|^2}{Z} \tag{3-15}$$

where Z is the intrinsic impedance of the propagation medium.

In matrix notation the power transferred from the incident wave to matched loads fed by feeds 1 and 2 is

$$\begin{bmatrix} P_1 \\ \\ P_2 \end{bmatrix} = \tfrac{1}{2}S \begin{bmatrix} Ae_1a_o & Ae_1a_1 & Ae_1a_2 & Ae_1a_3 \\ \\ Ae_2b_o & Ae_2b_1 & Ae_2b_2 & Ae_2b_3 \end{bmatrix} \begin{bmatrix} s_o \\ s_1 \\ s_2 \\ s_3 \end{bmatrix} \tag{3-16}$$

P_1 and P_2 may also be calculated from E_1 and E_2 by the matrix approach of equation (3-3):

$$P_1 = V_1^R V_1^{R*} = |V_1^R|^2 \tag{3-17}$$

$$P_2 = V_2^R V_1^{R*} = |V_2^R|^2 \tag{3-18}$$

where

$$\begin{bmatrix} V_1^R \\ V_2^R \end{bmatrix} = \begin{bmatrix} S_{11}^R & S_{12}^R \\ S_{21}^R & S_{22}^R \end{bmatrix} \begin{bmatrix} E_1^R \\ E_2^R \end{bmatrix} \tag{3-19}$$

Combining equations (3-16), (3-17), and (3-19),

$$|S_{11}^R\ E_1^R + S_{12}^R\ E_2^R|^2 = \tfrac{1}{2}S\ (Ae_1a_os_o + Ae_1a_1s_1 + Ae_1a_2s_2 + Ae_1a_3s_3) \tag{3-20}$$

$$|S_{11}^R\ E_1^R + S_{12}^R\ E_2^R|^2 = \frac{Ae_1}{2Z}\{a_o(|E_1^R|^2 + |E_2^R|^2) + a_1(|E_1^R|^2 - |E_2^R|^2) + a_2(2|E_1^R||E_2^R|\cos\delta) + a_3(2|E_1^R||E_2^R|\sin\delta)\} \tag{3-21}$$

Now

$$|S_{11}^R\ E_1^R + S_{12}^R\ E_2^R|^2 = (S_{11}^R\ E_1^R + S_{12}^R\ E_2^R)(S_{11}^{R*}\ E_1^{R*} + S_{12}^{R*}\ E_2^{R*}) \tag{3-22}$$

and therefore, the left side of (3-21) becomes

$$|S_{11}^R|^2|E_1^R|^2 + |S_{12}^R|^2|E_2^R|^2 + S_{12}^R E_2^R S_{11}^{R*} E_1^{R*} + S_{11}^R E_1^R S_{12}^{R*} E_2^{R*} =$$

$$|S_{11}^R|^2\ |E_1^R|^2 + |S_{12}^R|^2|E_2^R|^2 + 2\ \text{Real}\ \{S_{12}^R S_{11}^R E_1^R E_2^R\} \tag{3-23}$$

If the left side of (3-21) as above is arranged by degree in $|E_1|$ and $|E_2|$ and set equal to the right side, the result is

$$|S_{11}^R|^2 = \frac{Ae_1}{2Z}(a_o + a_1) \tag{3-24}$$

$$|S_{12}|^2 = \frac{Ae_1}{2Z}(a_o - a_1) \tag{3-25}$$

$$2 \text{ Real } \{S_{12}S_{11}E_1^R E_2^R\} = \frac{Ae_1}{2Z} 2|E_1^R||E_2^R|\{ a_2 \cos\delta + a_3 \sin\delta\} \tag{3-26}$$

The phase angle between E_1^R and E_2^R is δ. If we measure all phase angles with respect to E_1^R then

$$E_1^R E_2^R = |E_1^R||E_2^R|e^{j\delta}. \tag{3-27}$$

If

$$S_{12}^R = |S_{12}^R|e^{j\theta_{12}^R} \tag{3-28}$$

and

$$S_{11}^R = |S_{11}^R|e^{j\theta_{11}^R} \tag{3-29}$$

then (3-25) becomes

$$2|S_{12}^R||S_{11}^R|\cos(\theta_{11}^R + \theta_{12}^R + \delta) = \frac{Ae_1}{z}(a_2 \cos\delta + a_3 \sin\delta) \tag{3-30}$$

But

$$\cos(\theta_{11}^R + \theta_{12}^R + \delta) = \cos(\theta_{11}^R + \theta_{12}^R)\cos\delta - \sin(\theta_{11}^R + \theta_{12}^R)\sin\delta \tag{3-31}$$

and equating the multipliers of sin δ and cos δ on both sides of (3-30) yields

$$2|S_{12}^R||S_{11}^R|\cos(\theta_{11}^R + \theta_{12}^R) = \frac{a_2 Ae_1}{z} \tag{3-32}$$

$$2|S_{12}^R||S_{11}^R|\sin(\theta_{11}^R + \theta_{12}^R) = \frac{-a_3 Ae_1}{z} \tag{3-33}$$

Hence

$$\cos(\theta_{11}^R + \theta_{12}^R) = \frac{a_2}{2\sqrt{a_o^2 - a_1^2}} \tag{3-34}$$

$$\sin(\theta_{11}^R + \theta_{12}^R) = \frac{-a_3}{2\sqrt{a_o^2 - a_1^2}} \tag{3-35}$$

and

$$\theta_{11}^R + \theta_{12}^R = \cos^{-1}\frac{a_2}{2\sqrt{a_o^2 - a_1^2}} \tag{3-36}$$

$$\theta_{11}^R + \theta_{12}^R = \sin^{-1}\frac{-a_3}{2\sqrt{a_o^2 - a_1^2}} \tag{3-37}$$

Equations (3-36) and (3-37) define $\theta_{11}^R + \theta_{12}^R$ uniquely - i.e. without quadrant ambiguity.

In equations (3-36) and (3-37) the sum of θ_{11}^R and θ_{12}^R is determined rather than the individual phase angles themselves. This is immaterial to any calculations of received power, because by (3-23) and (3-27)

through (3-29) the received power in polarization 1 depends on the sum of Θ_{11}^R and Θ_{12}^R rather than on the individual angles. Hence Θ_{11}^R may arbitrarily set to zero without loss of generality.

The quantities S_{21}^R and S_{22}^R may be determined from the power received in polarization 2. Here,

$$P_2 = |S_{21}^R E_1^R + S_{22}^R E_2^R|^2 = \tfrac{1}{2}S\ (Ae_2 b_o s_o + Ae_2 b_1 s_1 + Ae_2 b_2 s_2 + Ae_2 b_3 s_3) \tag{3-38}$$

$$|S_{21}^R|^2 |E_1^R|^2 + |S_{22}^R|^2 |E_2^R|^2 + 2\ \text{Real}\ \{S_{21}^R S_{22}^R E_1^R E_2^R\} = \tfrac{1}{2}S\ (Ae_2 b_o s_o + Ae_2 b_1 s_1 + Ae_2 b_2 s_2 + Ae_2 b_3 s_3) \tag{3-39}$$

and

$$|S_{21}^R|^2 = \frac{Ae_1}{2z}\ (b_o + b_1) \tag{3-40}$$

$$|S_{22}^R|^2 = \frac{Ae_1}{2z}\ (b_o - b_1) \tag{3-41}$$

$$\Theta_{21}^R + \Theta_{22}^R = \cos^{-1} \frac{b_2}{2\sqrt{b_o^2 - b_1^2}} \tag{3-42}$$

$$\Theta_{11}^R + \Theta_{12}^R = \sin^{-1} \frac{b_1}{2\sqrt{b_o^2 - b_1^2}} \tag{3-43}$$

Thus, the receiving antenna transfer matrix elements may be derived from the normalized Stokes parameters.

3.2.2.2 Transmitting Antennas. The published gain and polarization characteristics of most transmitting antennas are inadequate to define numerical values for all elements of the transmitting antenna transfer matrix; these elements may be obtained by measurement or from the Stokes parameters via the transfer matrix for the same antenna when used in reception. Since the antenna is reciprocal, if applied normalized voltages $\begin{pmatrix} V_1 \\ V_2 \end{pmatrix}$ give rise to transmitted E field components $\begin{pmatrix} E_1 \\ E_2 \end{pmatrix}$, then under receiving conditions incident E field components $\begin{pmatrix} E_1 \\ E_2 \end{pmatrix}$ will produce received normalized voltages $\begin{pmatrix} V_1 \\ V_2 \end{pmatrix}$. Under transmitting conditions

$$\begin{bmatrix} E_1 \\ E_2 \end{bmatrix} = \begin{bmatrix} S_{11}^T & S_{12}^T \\ S_{21}^T & S_{22}^T \end{bmatrix} \begin{bmatrix} V_1 \\ V_2 \end{bmatrix} \qquad (3\text{-}44)$$

Multiplying both sides of (3-44) by the inverse of the transmitting transfer matrix and rearranging yields

$$\begin{bmatrix} V_1 \\ V_2 \end{bmatrix} = \begin{bmatrix} S_{11}^T & S_{12}^T \\ S_{21}^T & S_{22}^T \end{bmatrix}^{-1} \begin{bmatrix} E_1 \\ E_2 \end{bmatrix} \qquad (3\text{-}45)$$

Comparing (3-45) with the receiving antenna equation (3-4), the relationship between the transmitting and receiving transfer matrices for the same antenna is

$$\begin{bmatrix} S_{11}^R & S_{12}^R \\ S_{21}^R & S_{22}^R \end{bmatrix} = \begin{bmatrix} S_{11}^T & S_{12}^T \\ S_{21}^T & S_{22}^T \end{bmatrix}^{-1} \tag{3-46}$$

or, since the receiving matrix elements are assumed to be known,

$$\begin{bmatrix} S_{11}^T & S_{12}^T \\ S_{21}^T & S_{22}^T \end{bmatrix} = \begin{bmatrix} S_{11}^R & S_{12}^R \\ S_{21}^R & S_{22}^R \end{bmatrix}^{-1} \tag{3-47}$$

and in terms of the individual elements

$$S_{11}^T = \frac{S_{22}^R}{S_{11}^R S_{22}^R - S_{12}^R S_{21}^R} \tag{3-48}$$

$$S_{12}^T = \frac{-S_{12}^R}{S_{11}^R S_{22}^R - S_{12}^R S_{21}^R} \tag{3-49}$$

$$S_{21}^T = \frac{-S_{21}^R}{S_{11}^R S_{22}^R - S_{12}^R S_{21}^R} \tag{3-50}$$

$$S_{22}^T = \frac{S_{11}^R}{S_{11}^R S_{22}^R - S_{12}^R S_{21}^R} \tag{3-51}$$

The receiving transfer matrix elements can be calculated from the Stokes parameters.

3.2.2.3 A Comparison of Receiving Antenna and Transmitting Antenna Characteristics. The absolute magnitudes of the transmitting antenna parameters in (3-48) through (3-51) are all considerably smaller than the absolute magnitude of the corresponding receiving parameters. At first, the result is surprising, but if one remembers that in this representation the antenna is described as a four-port reciprocal network, analogies come to mind. In a four-port network for example, if a 1 volt source at port 1 delivers 100 volts at port 3 ("forward" transfer function of 100), then a 100 volt source at port 3 will deliver 1 volt to the same load at port 1 ("reverse" transfer function of 0.01). The relative magnitude of the transfer matrix elements ($|S_{12}|/|S_{22}|$ etc.) is essentially the same for either transmission or reception.

If (as generally will be true for good antennas)

$$|S_{11}| >> |S_{12}|$$

$$|S_{11}| >> |S_{21}|$$

and

$$S_{11} \simeq S_{22}$$

then

$$S_{11}^T \simeq 1/S_{22}^R \qquad (3\text{-}52)$$

$$S_{22}^T \simeq 1/S_{11}^R \qquad (3\text{-}53)$$

3.3 Cross Polarization Isolation and Discrimination

There are two useful definitions of cross polarization level that may be applied to a system capable of transmitting and receiving signals on two orthogonal polarization. According to Watson [1973] these are:

(a) cross polarization isolation - the ratio of the power received in one receiver channel from the co-polarized transmitter channel to the power received from the cross-polarized transmitter channel.

(b) cross polarization discrimination - the ratio of the power received in one receiver channel from the co-polarized transmitter channel to the power received in the cross polarized receiver channel from the same transmitter channel.

In the notation of this report these quantities are given by

$$I_{12} = 20 \log_{10} \left| \frac{V_2^R \text{ for } V_2^T = 1 \text{ and } V_1^T = 0}{V_2^R \text{ for } V_2^T = 0 \text{ and } V_1^T = 1} \right| \tag{3-54}$$

$$I_{12} = 20 \log_{10} \left| \frac{S_{21}^R S_{11}^P S_{12}^T + S_{21}^R S_{12}^P S_{22}^T + S_{22}^R S_{21}^P S_{12}^T + S_{22}^R S_{22}^P S_{22}^T}{S_{21}^R S_{11}^P S_{11}^T + S_{21}^R S_{12}^P S_{21}^T + S_{22}^R S_{21}^P S_{11}^T + S_{22}^R S_{22}^P S_{21}^T} \right| \tag{3-55}$$

$$I_{21} = 20 \log_{10} \left| \frac{V_1^R \text{ for } V_1^T = 1 \text{ and } V_2^T = 0}{V_1^R \text{ for } V_1^T = 0 \text{ and } V_2^T = 1} \right| \tag{3-56}$$

$$I_{21} = 20 \log_{10} \left| \frac{S_{11}^R S_{11}^P S_{11}^T + S_{11}^R S_{12}^P S_{21}^T + S_{12}^R S_{21}^P S_{11}^T + S_{12}^R S_{22}^P S_{21}^T}{S_{11}^R S_{11}^P S_{12}^T + S_{11}^R S_{12}^P S_{22}^T + S_{12}^R S_{21}^P S_{12}^T + S_{12}^R S_{22}^P S_{22}^T} \right| \tag{3-57}$$

$$D_{21} = 20 \log_{10} \left| \frac{V_2^R \text{ for } V_2^T = 1,\ V_1^T = 0}{V_1^R \text{ for } V_2^T = 1,\ V_1^T = 0} \right| \tag{3-58}$$

$$D_{21} = 20 \log_{10} \left| \frac{S_{21}^R S_{11}^P S_{12}^T + S_{21}^R S_{12}^P S_{22}^T + S_{22}^R S_{21}^P S_{12}^T + S_{22}^R S_{22}^P S_{22}^T}{S_{11}^R S_{11}^P S_{12}^T + S_{11}^R S_{12}^P S_{22}^T + S_{12}^R S_{21}^P S_{12}^T + S_{12}^R S_{22}^P S_{22}^T} \right| \tag{3-59}$$

$$D_{12} = 20 \log_{10} \left| \frac{V_1^R \text{ for } V_1^T = 1,\ V_2^T = 0}{V_2^R \text{ for } V_1^T = 1,\ V_2^T = 0} \right| \tag{3-60}$$

$$D_{12} = 20 \log_{10} \left| \frac{S_{11}^R S_{11}^P S_{11}^T + S_{11}^R S_{12}^P S_{21}^T + S_{12}^R S_{21}^P S_{11}^T + S_{12}^R S_{22}^P S_{21}^T}{S_{21}^R S_{11}^P S_{11}^T + S_{21}^R S_{12}^P S_{21}^T + S_{22}^R S_{21}^P S_{11}^T + S_{22}^R S_{22}^P S_{21}^T} \right| \tag{3-61}$$

where I indicates isolation and D indicates discrimination.

The question naturally arises as to whether discrimination and isolation may be equal. Watson [1973] has shown that <u>for the propagation medium alone</u> (<u>i.e.</u> for ideal antennas) $I_{12} = D_{21}$ and $I_{21} = D_{12}$. However, for a complete communications system with non-ideal antennas equality of I_{12} and D_{21} requires that

$$\left| S_{21}^R S_{11}^P S_{11}^T + S_{21}^R S_{12}^P S_{21}^T + S_{22}^R S_{21}^P S_{11}^T + S_{22}^R S_{22}^P S_{21}^T \right| = \left| S_{11}^R S_{11}^P S_{12}^T + S_{11}^R S_{12}^P S_{22}^T + S_{12}^R S_{21}^P S_{12}^T + S_{12}^R S_{22}^P S_{22}^T \right| \tag{3-62}$$

and (3-62) would be satisfied only randomly because of the phase fluctuations and path terms.

3.4 The Theoretical Behavior of System Cross Polarization Isolation

3.4.1 Introduction

This section explores the theoretical behavior of the cross polarization isolation of a complete system (i.e. transmitting antenna, propagation path, and receiving antenna) and contrasts it with the prediction theories which consider the propagation medium alone.

3.4.2 Reciprocity

In antenna theory the practical meaning of reciprocity is that in any communications system the transmitting and receiving antennas can be interchanged (so long as each antenna "sees" a conjugate impedance match before and after the interchange) without affecting the received signal strength. Reciprocity is a property of antennas operating in an isotropic environment but not of antennas operating in an anisotropic environment.

If rain can be modeled as an ensemble of ellipsoids with a mean orientation of major and minor axes, the E field of a propagating linearly polarized wave will rotate toward the mean minor axis of the drop population, irrespective of the direction of propagation. Hence, rain is as anisotropic as any medium which induces polarization rotation -- the ferrite in a Faraday rotation isolator, for instance. This means that, in general, the strengths of signals passing through rain will depend on the direction of propagation and hence, on the identity of the transmitting and receiving antennas.

To illustrate this absence of reciprocity, imagine a linearly polarized system using ideal antennas with a propagation path directed along the Z axis. Let antenna #1 be polarized along the X axis and let

antenna #2 be polarized at an angle of 2^{o} toward the +Y axis with respect to the X axis. Assume that rain induces a 2^{o} rotation toward the +Y axis. When antenna #1 transmits and antenna #2 receives, the rain polarization rotation exactly compensates for the antenna misalignment and no cross polarization is measured. But when antenna #2 transmits and antenna #1 receives, the received E field is 4^{o} out of alignment with the receiving antenna and significant cross polarization is measured. Hence, observed cross polarization levels can depend on the direction of propagation and reciprocity does not hold. This effect is a property of the antennas used and it is not included in theories which describe the propagation medium only.

3.4.3 The Effects of Rain Depolarization on Isolation

In any dual-polarized communications system cross polarized signal components are measured in clear weather because of unavoidable imperfections in antenna alignment and construction. This residual cross polarization imposes a limit on the minimum obtainable communications system crosstalk and - surprisingly - on the accuracy with which rain depolarization can be measured. At the start of this investigation our guess was that the residual cross polarization would set some sort of system sensitivity threshold and that as soon as rain depolarization exceeded this threshold, our system would measure the rain depolarization directly with good accuracy. This does not seem to be true; as the discussion to follow indicates, rain depolarization will change the isolation of any communications system but the depolarization due to rain must be substantially greater than the

residual cross polarization level if the observed polarization isolation is to match that predicted by theory for the propagation medium alone.

The residual or clear weather cross polarizations I_{12}^0 and I_{21}^0 may be obtained from equations (3-55) and (3-57) by setting the path terms S_{12}^P and S_{21}^P to zero. The results are

$$I_{12}^0 = 20 \log_{10} \left| \frac{S_{21}^R S_{11}^{PO} S_{12}^T + S_{22}^R S_{22}^{PO} S_{22}^T}{S_{21}^R S_{11}^{PO} S_{11}^T + S_{22}^R S_{22}^{PO} S_{21}^T} \right| \tag{3-63}$$

$$I_{21}^0 = 20 \log_{10} \left| \frac{S_{11}^R S_{11}^{PO} S_{11}^T + S_{12}^R S_{22}^{PO} S_{21}^T}{S_{11}^R S_{11}^{PO} S_{12}^T + S_{12}^R S_{22}^{PO} S_{22}^T} \right| \tag{3-64}$$

In (3-63) and (3-64) the 0 in S_{11}^{PO} and S_{22}^{PO} indicates clear-weather values.

Now in clear weather the propagation medium is of necessity isotropic and $S_{11}^{PO} = S_{22}^{PO} = S^{PO}$ and these terms may be cancelled from (3-63) and (3-64). In addition, for good antennas $|S_{11}|$ and $|S_{22}|$ should be much larger than $|S_{12}|$ or $|S_{21}|$ and this may be used to simplify the numerators of (3-63) and (3-64). The results of these changes are:

$$I_{12}^0 = 20 \log_{10} \left| \frac{S_{22}^T}{S_{21}^R + S_{21}^T} \right| \tag{3-65}$$

$$I_{21}^0 = 20 \log_{10} \left| \frac{S_{11}^T}{S_{12}^R + S_{12}^T} \right| \tag{3-66}$$

Equations (3-65) and (3-66) are invariant with an interchange of transmitting and receiving antennas. They must be, since reciprocity holds for clear-weather conditions.

Without loss of generality, all of the antenna depolarization can be lumped into one antenna and the other antenna treated as ideal. Thus, assume that $S_{21}^R = S_{12}^R = 0$ (*i.e.* the receiving antenna is ideal) and that

$$I_{12}^0 = 20 \log_{10} \left| \frac{S_{22}^T}{S_{21}^T} \right| \tag{3-67}$$

$$I_{21}^0 = 20 \log_{10} \left| \frac{S_{11}^T}{S_{12}^T} \right| \tag{3-68}$$

Hence,

$$\left| \frac{S_{21}^T}{S_{22}^T} \right| = 10\, e^{-(I_{12}^0/20)} \tag{3-69}$$

$$\left| \frac{S_{12}^T}{S_{11}^T} \right| = 10\, e^{-(I_{21}^0/20)} \tag{3-70}$$

Now look at the effect that I_{12}^0 and I_{21}^0 have on observed cross polar isolation during rain. Under the above assumption that $S_{21}^R = S_{12}^R = 0$,

$$I_{12} = 20 \log_{10} \left| \frac{S_{21}^P S_{12}^T + S_{22}^P S_{22}^T}{S_{21}^P S_{11}^T + S_{22}^P S_{21}^T} \right| \tag{3-71}$$

$$I_{21} = 20 \log_{10} \left| \frac{S_{11}^P S_{11}^T + S_{12}^P S_{21}^T}{S_{11}^P S_{12}^T + S_{12}^P S_{22}^T} \right| \tag{3-72}$$

Again, $|S_{22}^P S_{22}^T| >> |S_{21}^P S_{12}^T|$ and $|S_{11}^P S_{11}^T| >> |S_{12}^P S_{21}^T|$ and

$$I_{12} \simeq 20 \log_{10} \left| \frac{S_{22}^P S_{22}^T}{S_{21}^P S_{11}^T + S_{22}^P S_{21}^T} \right| \tag{3-73}$$

$$I_{21} \simeq 20 \log_{10} \left| \frac{S_{11}^P S_{11}^T}{S_{11}^P S_{12}^T + S_{12}^P S_{22}^T} \right| \tag{3-74}$$

Under ideal conditions $S_{12}^T = S_{21}^T = 0$ and $S_{11}^T = S_{22}^T$ and

$$I_{12} = I_{12}^P = 20 \log_{10} \left| \frac{S_{22}^P}{S_{21}^P} \right| \tag{3-75}$$

$$I_{21} = I_{21}^P = 20 \log_{10} \left| \frac{S_{11}^P}{S_{12}^P} \right| \tag{3-76}$$

where I_{12}^P and I_{21}^P are the cross polar isolations of the propagation medium itself. Under real conditions it is still reasonable to assume that $S_{11}^T = S_{22}^T$. Hence,

$$I_{12} = 20 \log_{10} |S^P_{22}| - 20 \log_{10} \left| S^P_{22} \frac{S^T_{21}}{S^T_{22}} + S^P_{21} \right| \quad (3\text{-}77)$$

$$I_{21} = 20 \log_{10} |S^P_{11}| - 20 \log_{10} \left| S^P_{11} \frac{S^T_{12}}{S^T_{22}} + S^P_{12} \right| \quad (3\text{-}78)$$

In each of the above equations the first term is well defined and easy to evaluate. But in each case, the second term involves four complex numbers whose magnitudes are well known but whose phase angles are not. It is possible to treat extreme cases - i.e. I_{12} must lie between I^A_{12} and I^B_{12}, where

$$I^A_{12} = 20 \log_{10} |S^P_{22}| - 20 \log_{10} \left| \left| \frac{S^P_{22} S^T_{21}}{S^T_{22}} \right| + |S^P_{21}| \right| \quad (3\text{-}79)$$

$$I^B_{12} = 20 \log_{10} |S^P_{22}| - 20 \log_{10} \left| \left| \frac{S^P_{22} S^T_{21}}{S^T_{22}} \right| - |S^P_{21}| \right| \quad (3\text{-}80)$$

Similarly, I_{21} must be between I^A_{21} and I^B_{21} where

$$I^A_{21} = 20 \log_{10} |S^P_{11}| - 20 \log_{10} \left| \left| \frac{S^P_{11} S^T_{12}}{S^T_{22}} \right| + |S^P_{12}| \right| \quad (3\text{-}81)$$

$$I^B_{21} = 20 \log_{10} |S^P_{11}| - 20 \log_{10} \left| \left| \frac{S^P_{11} S^T_{12}}{S^T_{22}} \right| - |S^P_{12}| \right| \quad (3\text{-}82)$$

For a numerical example, consider the path and antennas used in this project.

$$S^{PO} = 120.48 \text{ dB or } 9.4624 \times 10^{-7}$$

Assume that one channel has a residual isolation of 30 dB and the other has a residual isolation of 50 dB. Then

$$I_{12}^{O} = 50 \text{ dB},$$

$$\left|\frac{S_{21}^{T}}{S_{22}^{T}}\right| = 10^{-5/2} = 3.1623 \times 10^{-3},$$

and

$$I_{21}^{O} = 30 \text{ dB},$$

$$\left|\frac{S_{12}^{T}}{S_{22}^{T}}\right| = 10^{-3/2} = 3.1623 \times 10^{-2}$$

For 45° linear polarization (and 0° canting angle) a table of cross polarization levels for each rain fall rate may be constructed using S_{11}^{P} and S_{12}^{P} as predicted by the scattering model. See Table 3.1 as an example.

The average values of I_{12} and I_{21} are also of great interest. To get them, note that the last terms in Equations (3-77) and (3-78) represent the power in the received cross polarized signal expressed in dBW. If the two phasors $\frac{S_{22}^{P} S_{21}^{T}}{S_{22}^{T}}$ and S_{21}^{P} are uncorrelated and their phase angles have a uniform probability density, they add incoherently and the average power in the sum of the two phasors is the sum of the average power in each phasor. Thus, in (3-77)

Table 3-1 Limiting Values of Isolation During Rain for Clear Weather Isolations Assumed in Text

Rain Rate (mm/hr)	$\lvert S_{11}^P \rvert$ and $\lvert S_{22}^P \rvert \times 10^7$	$\lvert S_{12}^P \rvert$ and $\lvert S_{21}^P \rvert \times 10^8$	I_{12}^A dB	I_{21}^A dB	I_{12}^B dB	I_{21}^B dB	I_{12}^P, I_{21}^P dB
10	8.0967	0.58649	39.65	28.21	47.78	32.26	42.8
30	5.8445	1.5540	30.53	24.70	32.61	45.96	31.51
50	4.2067	2.2184	25.05	20.80	28.95	36.37	25.56
70	3.0224	2.4905	21.35	18.86	22.02	25.89	21.68
90	2.1694	2.4739	18.86	16.73	21.98	24.56	18.86
110	1.5563	2.2867	16.47	14.96	16.85	18.76	16.66
130	1.1162	2.0171	14.71	13.46	15.01	16.53	14.86
150	0.80065	1.7224	13.22	12.16	13.47	14.73	13.34

$$\left\langle \left| \frac{S_{22}^P S_{21}^T}{S_{22}^T} + S_{21}^P \right|^2 \right\rangle = \left| \frac{S_{22}^P S_{21}^T}{S_{22}^T} \right|^2 + |S_{21}^P|^2 \qquad (3\text{-}83)$$

and the average value of I_{12} becomes

$$\langle I_{12} \rangle = 20 \log_{10} |S_{22}^P| - 10 \log_{10} \left(\left| \frac{S_{22}^P S_{21}^T}{S_{22}^T} \right|^2 + |S_{21}^P|^2 \right) \qquad (3\text{-}84)$$

Similarly for I

$$\langle I_{21} \rangle = 20 \log_{10} |S_{11}^P| - 10 \log_{10} \left(\left| \frac{S_{11}^P S_{12}^T}{S_{22}^T} \right|^2 + |S_{12}^P|^2 \right) \qquad (3\text{-}85)$$

In any measurement of I_{12}, the observed values should fall between I_{12}^A and I_{12}^B with a mean of $\langle I_{12} \rangle$.

Figure 3-1 illustrates the expected variation of I_{12} with rainfall rate for selected values of I_{12}^0, assuming $\pm 45^\circ$ linear polarization, a canting angle of 0°, and a 19.3 GHz path used in this project. The propagation medium isolation I_{12}^P is also shown. Tables 3-2, 3-3, and 3-4 list values of average, minimum, and maximum cross polarization isolation as functions of clear weather isolation and rain rate.. For low values of clear weather isolation, the cross polarization isolation of a complete system is significantly worse than that of the rain-filled path alone. Both antenna and rain effects must be considered in system design.

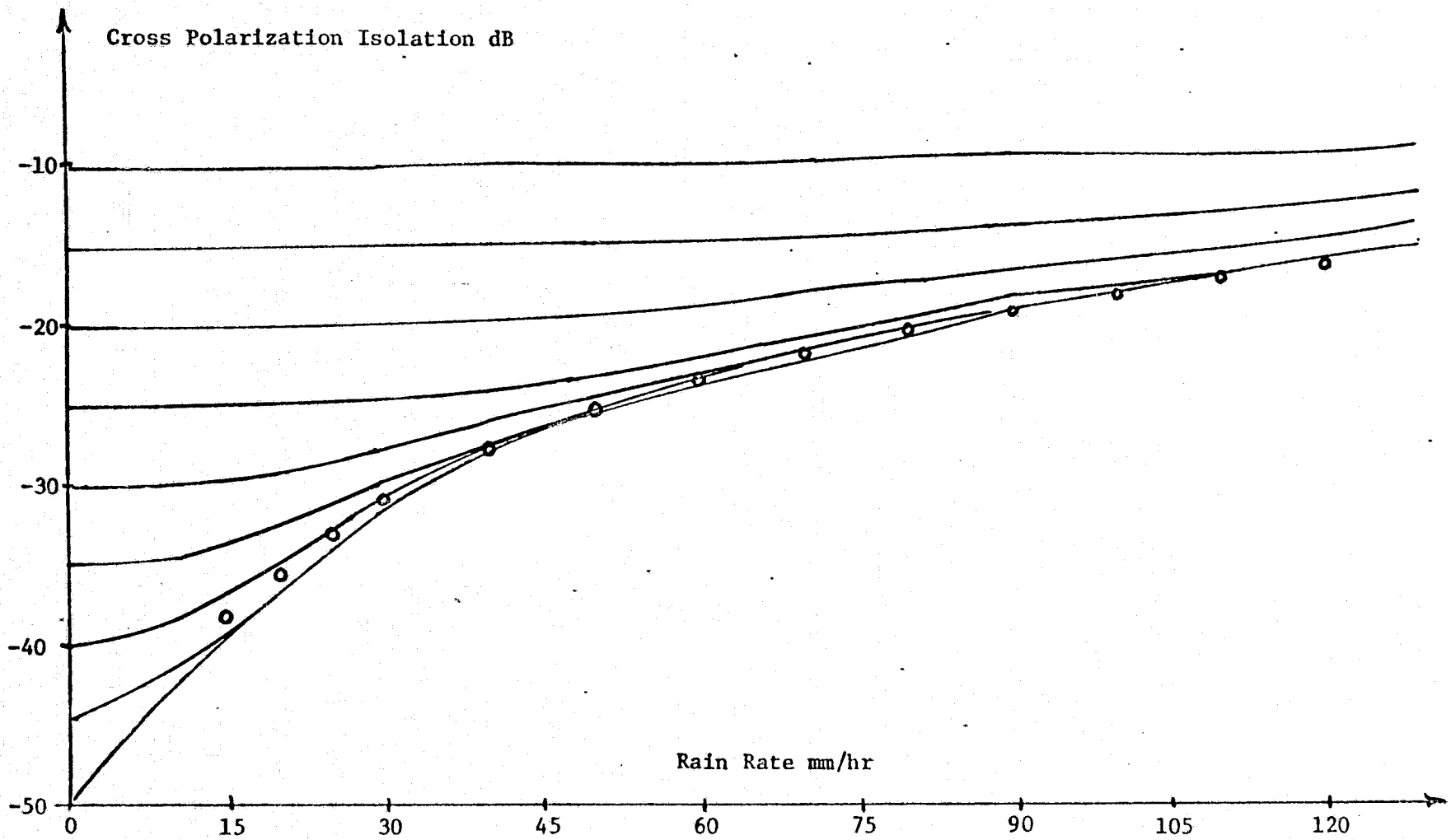

Figure 3-1 Cross polarization isolation versus rain rate for systems with different clear weather isolations. Dots indicate isolation of the propagation medium alone. Path length is 1.43 km, frequency is 17.65 GHz, and polarization is 45° linear.

Table 3-2 Average Isolation I as a Function of Clear Weather Isolation and Rain Rate for ±45° Linear Polarization at 19.3 GHz Along a 1.43 Km Path

CW ISOL	R=10	R=30	R=50	R=70	R=90	R=110	R=120	R=150
50.00	42.04	31.44	25.54	21.67	18.86	16.66	14.86	13.35
49.00	41.87	31.43	25.54	21.67	18.85	16.66	14.86	13.35
48.00	41.65	31.41	25.53	21.67	18.85	16.65	14.86	13.34
47.00	41.40	31.39	25.53	21.67	18.85	16.65	14.86	13.34
46.00	41.10	31.35	25.52	21.67	18.85	16.65	14.86	13.34
45.00	40.75	31.32	25.51	21.66	18.85	16.65	14.86	13.34
44.00	40.35	31.27	25.50	21.66	18.85	16.65	14.86	13.34
43.00	39.89	31.21	25.48	21.65	18.84	16.65	14.85	13.34
42.00	39.37	31.13	25.46	21.64	18.84	16.65	14.85	13.34
41.00	38.80	31.04	25.44	21.63	18.83	16.64	14.85	13.34
40.00	38.17	30.93	25.40	21.62	18.83	16.64	14.85	13.34
39.00	37.49	30.79	25.37	21.60	18.82	16.63	14.84	13.33
38.00	36.76	30.63	25.32	21.58	18.81	16.63	14.84	13.33
37.00	35.99	30.43	25.26	21.56	18.79	16.62	14.83	13.33
36.00	35.18	30.19	25.18	21.52	18.78	16.61	14.83	13.32
35.00	34.33	29.90	25.09	21.48	18.75	16.59	14.82	13.32
34.00	33.46	29.57	24.98	21.43	18.73	16.58	14.81	13.31
33.00	32.57	29.19	24.84	21.37	18.67	16.56	14.79	13.30
32.00	31.65	28.74	24.67	21.30	18.65	16.53	14.78	13.29
31.00	30.72	28.24	24.47	21.20	18.60	16.50	14.76	13.27
30.00	29.78	27.68	24.22	21.08	18.54	16.46	14.73	13.25
29.00	28.82	27.06	23.94	20.94	18.46	16.41	14.70	13.23
28.00	27.86	26.40	23.60	20.77	18.36	16.35	14.65	13.20
27.00	26.89	25.68	23.21	20.56	18.24	16.27	14.60	13.16
26.00	25.91	24.92	22.76	20.31	18.09	16.18	14.54	13.12
25.00	24.93	24.12	22.26	20.02	17.91	16.06	14.46	13.06
24.00	23.94	23.29	21.70	19.68	17.70	15.92	14.36	12.99
23.00	22.95	22.43	21.08	19.28	17.44	15.75	14.24	12.90
22.00	21.96	21.54	20.41	18.83	17.14	15.54	14.09	12.79
21.00	20.97	20.63	19.70	18.32	16.79	15.30	13.91	12.66
20.00	19.98	19.70	18.93	17.75	16.38	15.00	13.70	12.50
19.00	18.98	18.76	18.13	17.13	15.92	14.66	13.44	12.30
18.00	17.99	17.81	17.30	16.45	15.40	14.27	13.14	12.07
17.00	16.99	16.85	16.43	15.73	14.82	13.82	12.79	11.79
16.00	15.99	15.88	15.54	14.96	14.19	13.31	12.38	11.46
15.00	14.99	14.90	14.63	14.16	13.50	12.74	11.92	11.08
14.00	13.99	13.92	13.71	13.32	12.77	12.12	11.40	10.65
13.00	13.00	12.94	12.77	12.45	12.00	11.44	10.82	10.16
12.00	12.00	11.95	11.81	11.56	11.19	10.72	10.19	9.61
11.00	11.00	10.96	10.85	10.64	10.34	9.96	9.50	9.01
10.00	10.00	9.97	9.88	9.71	9.47	9.15	8.77	8.35
9.00	9.00	8.98	8.91	8.77	8.57	8.31	8.00	7.64
8.00	8.00	7.98	7.92	7.82	7.66	7.45	7.19	6.89
7.00	7.00	6.98	6.94	6.85	6.73	6.55	6.34	6.09
6.00	6.00	5.99	5.95	5.88	5.78	5.64	5.47	5.27
5.00	5.00	4.99	4.96	4.91	4.82	4.71	4.57	4.41
4.00	4.00	3.99	3.97	3.93	3.86	3.77	3.66	3.52
3.00	3.00	2.99	2.98	2.94	2.89	2.82	2.73	2.62
2.00	2.00	2.00	1.98	1.95	1.91	1.85	1.78	1.69
1.00	1.00	1.00	0.98	0.96	0.93	0.88	0.83	0.75
0.00	-0.00	-0.00	-0.01	-0.03	-0.06	-0.09	-0.14	-0.20

Table 3-3 Minimum Isolation I^A as a Function of Clear Weather Isolation and Rain Rate for ±45° Linear Polarization at 19.3 GHz Along a 1.43 Km Path

CW ISOL UPPER LIMITS	R=10	R=30	R=50	R=70	R=90	R=110	R=130	R=150
50.00	39.62	30.53	25.05	21.5[illegible]	18.62	16.47	14.71	13.27
[illegible]	39.34	[illegible].42	24.99	21.32	19.59	16.4[illegible]	14.69	13.20
[illegible]	[illegible]	[illegible]	24.63	21.27	18.56	16.43	14.67	13.19
47.00	38.63	30.10	24.85	21.22	18.53	16.40	14.65	13.17
[illegible].00	38.23	30.01	24.77	21.17	18.49	16.37	14.62	13.15
[illegible]	37.81	29.84	24.68	21.11	18.44	16.33	14.59	13.12
[illegible]	37.36	29.66	24.58	21.04	18.39	16.29	14.56	13.1[illegible]
[illegible]	[illegible]	29.46	24.46	20.97	18.34	16.25	14.53	13.0[illegible]
[illegible]	36.37	29.24	24.34	20.88	18.27	16.20	14.49	13.02
[illegible]	[illegible]	29.00	24.21	20.79	18.21	16.15	14.44	12.99
40.00	35.27	28.73	24.05	20.69	18.13	16.09	14.39	12.95
39.00	34.67	28.42	23.88	20.57	18.04	16.02	14.34	12.90
38.00	34.05	28.14	23.70	20.45	17.95	15.94	14.28	12.85
37.00	33.40	27.81	23.50	20.31	17.84	15.86	14.21	12.79
36.00	32.73	27.44	23.28	20.15	17.73	15.77	14.13	12.73
35.00	32.03	27.06	23.03	19.98	17.60	15.67	14.05	12.66
34.00	31.31	26.64	22.77	19.81	17.46	15.55	13.95	12.58
33.00	30.57	26.20	22.48	19.62	17.31	15.43	13.85	12.49
32.00	29.80	25.73	22.17	19.37	17.13	15.29	13.73	12.39
31.00	29.01	25.23	21.84	19.13	16.94	15.13	13.6	12.28
30.00	28.21	24.70	21.48	18.86	16.73	14.96	13.46	12.15
29.00	27.39	24.14	21.09	18.57	16.51	14.78	13.3[illegible]	12.02
28.00	26.55	23.56	20.67	18.26	16.26	14.56	13.1[illegible]	11.87
27.00	25.69	22.94	20.23	17.92	15.99	14.35	12.94	11.71
26.00	24.82	22.3[illegible]	19.76	17.56	15.69	14.11	12.73	11.5[illegible]
25.00	23.95	21.64	19.25	17.16	15.38	13.84	12.51	11.33
24.00	23.06	20.95	18.72	16.74	15.03	13.55	12.26	11.11
23.00	22.1[illegible]	20.23	18.16	16.3[illegible]	14.66	13.24	11.9[illegible]	10.8[illegible]
22.00	21.24	19.49	17.58	15.82	14.27	12.90	11.[illegible]7	10.[illegible]
21.00	20.3[illegible]	18.73	16.96	15.31	13.84	12.54	11.[illegible]	1[illegible]
20.00	19.39	17.95	16.32	14.72	13.39	12.15	11.[illegible]3	1[illegible]3
19.00	18.46	17.15	15.65	14.2	12.91	11.73	10.67	9.70
18.00	17.51	16.34	14.96	13.63	12.40	11.28	10.27	9.34
17.00	16.57	15.50	14.24	13.01	11.88	10.81	9.84	8.96
16.00	15.61	14.65	13.51	12.36	11.29	10.30	9.39	8.55
15.00	14.65	13.79	12.74	11.69	10.70	9.77	8.91	8.11
14.00	13.69	12.91	11.96	11.00	10.07	9.21	8.4[illegible]	7.65
13.00	12.72	12.03	11.16	10.28	9.42	8.62	7.86	7.15
12.00	11.75	11.13	10.34	9.5[illegible]	8.75	8.00	7.29	6.63
11.00	10.78	10.22	9.51	8.77	8.09	7.36	6.7[illegible]	6.07
10.00	9.80	9.30	8.66	7.99	7.33	6.69	6.07	5.49
9.00	8.82	8.37	7.80	7.19	6.58	5.99	5.42	4.88
8.00	7.84	7.44	6.92	6.37	5.81	5.27	4.75	4.25
7.00	6.86	6.50	6.03	5.55	5.03	4.53	4.0[illegible]	3.59
6.00	5.3[illegible]	5.55	5.13	4.6[illegible]	4.22	3.77	3.3[illegible]	2.90
5.00	4.89	4.60	4.22	3.81	3.40	2.98	2.5[illegible]	2.19
4.00	3.9[illegible]	3.64	3.30	2.93	2.56	2.18	1.91	1.45
3.00	2.91	2.68	2.38	2.04	1.7[illegible]	1.36	1.0[illegible]	0.79
2.00	1.9[illegible]	1.71	1.44	1.14	0.8[illegible]	0.53	0.2[illegible]	−0.[illegible]
1.00	0.9[illegible]	0.74	0.50	0.2[illegible]	−0.05	−0.33	−0.6[illegible]	−0.[illegible]
0.0	−0.06	−0.23	−0.45	−0.[illegible]	−0.[illegible]	−1.[illegible]	−1.[illegible]	−1.[illegible]

Table 3-4 Maximum Isolation I^B as a Function of Clear Weather Isolation and Rain Rate for ±45° Linear Polarization at 19.3 GHz Along a 1.43 Km Path

CW ISOL LOWER LIMITS	R=10	R=30	R=50	R=70	R=90	R=110	R=130	R=150
50.00	47.78	32.61	26.10	22.02	19.10	16.85	15.01	13.47
49.00	48.65	32.75	26.16	22.06	19.13	16.87	15.03	13.49
48.00	49.73	32.91	26.24	22.11	19.17	16.90	15.05	13.51
47.00	51.13	33.10	26.33	22.17	19.21	16.93	15.08	13.53
46.00	53.03	33.32	26.43	22.23	19.25	16.96	15.10	13.55
45.00	55.81	33.57	26.54	22.30	19.30	17.00	15.13	13.58
44.00	60.59	33.86	26.66	22.37	19.35	17.04	15.17	13.60
43.00	75.70	34.20	26.81	22.46	19.42	17.09	15.21	13.64
42.00	63.10	34.59	26.98	22.56	19.49	17.14	15.25	13.67
41.00	55.55	35.05	27.17	22.68	19.57	17.20	15.30	13.71
40.00	51.19	35.60	27.38	22.81	19.66	17.27	15.35	13.76
39.00	48.01	36.27	27.64	22.95	19.76	17.35	15.42	13.81
38.00	45.44	37.08	27.93	23.12	19.88	17.44	15.49	13.87
37.00	43.25	38.09	28.27	23.31	20.01	17.54	15.57	13.94
36.00	41.30	39.38	28.66	23.54	20.16	17.65	15.66	14.01
35.00	39.51	41.13	29.13	23.79	20.33	17.78	15.76	14.10
34.00	37.92	43.56	29.69	24.09	20.53	17.93	15.88	14.19
33.00	36.40	47.53	30.36	24.43	20.76	18.09	16.01	14.30
32.00	34.93	56.65	31.18	24.84	21.02	18.29	16.16	14.42
31.00	33.56	55.95	32.20	25.32	21.32	18.51	16.33	14.57
30.00	32.26	45.96	33.51	25.89	21.68	18.76	16.53	14.73
29.00	31.03	41.32	35.26	26.57	22.10	19.06	16.76	14.91
28.00	29.74	37.57	37.77	27.41	22.59	19.40	17.02	15.12
27.00	28.54	34.66	41.87	28.47	23.19	19.81	17.33	15.37
26.00	27.36	32.57	51.65	29.82	23.89	20.28	17.68	15.65
25.00	26.20	31.38	49.12	31.64	24.76	20.85	18.10	15.98
24.00	25.06	28.71	39.69	34.29	25.86	21.53	18.59	16.36
23.00	23.94	27.09	34.87	38.71	27.28	22.37	19.18	16.81
22.00	22.83	25.54	31.47	56.55	29.22	23.41	19.89	17.35
21.00	21.74	24.06	28.78	43.45	32.07	24.76	20.76	17.99
20.00	20.65	22.68	26.51	35.09	37.06	26.57	21.86	18.78
19.00	19.58	21.35	24.51	30.52	54.73	29.19	23.28	19.75
18.00	18.51	20.08	22.71	27.23	38.52	33.54	25.22	20.99
17.00	17.46	18.81	21.05	24.60	31.30	44.92	28.08	22.63
16.00	16.41	17.66	19.51	22.37	27.04	36.74	33.06	24.94
15.00	15.36	16.41	18.06	20.41	23.90	30.20	50.80	28.57
14.00	14.32	15.24	16.67	18.63	21.36	25.58	34.51	36.14
13.00	13.29	14.11	15.33	16.99	19.19	22.28	27.30	41.16
12.00	12.25	13.07	14.05	15.45	17.26	19.64	23.04	28.86
11.00	11.23	11.98	12.80	14.00	15.50	17.40	19.90	23.52
10.00	10.21	10.71	11.58	12.62	13.88	15.43	17.36	19.90
9.00	9.18	9.58	10.40	11.30	12.37	13.84	15.16	17.10
8.00	8.16	8.60	9.23	10.01	10.93	12.00	13.25	14.75
7.00	7.14	7.59	8.09	8.77	9.56	10.46	11.50	12.71
6.00	6.13	6.47	6.97	7.56	8.24	9.01	9.88	10.87
5.00	5.11	5.42	5.86	6.38	6.97	7.63	8.37	9.19
4.00	4.10	4.37	4.76	5.22	5.73	6.30	6.93	7.62
3.00	3.09	3.33	3.67	4.07	4.53	5.02	5.56	6.15
2.00	2.08	2.30	2.60	2.95	3.35	3.78	4.24	4.74
1.00	1.07	1.26	1.53	1.84	2.19	2.56	2.97	3.40
0.00	0.08	0.23	0.47	0.75	1.05	1.38	1.73	2.10

4. Experimental Results

4.1 Introduction

Chapter 2 described the theory of millimeter wave rain depolarization and Chapter 3 explored its effect on the interchannel isolation of a dual-polarized radio communications system. This chapter summarizes the experimental data collected in the project and discusses the agreement of theory with experiment.

4.2 General Guide to the Data

4.2.1 Collection

The basic data recorded for all storms were:

(a) rainfall rate (measured by time between tips) at each rain gauge,

(b) co-polarized signal levels, and

(c) cross polarized signal levels.

For some storms we also recorded:

(a) wind speed and direction at one or two locations along the path and

(b) the IF phase difference between the receiver channels.

All data were initially recorded in the PB-440 computer memory and later forwarded to an IBM 370/155 or 370/158 system for analysis and display. For each storm the 370 received rain rates from each gauge plus quasi-instantaneous (i.e. 0.4 second integration time) samples of all analog signals. The latter were stored at essentially regular

times while the time intervals between successive rain gauge trips were random. Before comparing data taken from different inputs at different times the computer had to generate a time-function representation for each data variable. These time functions were then averaged over appropriate time intervals to generate the average signal levels, rain rates, etc. required by steady-state theory.

In generating the time functions, the computer first constructed a table of values and entry times for each data input active during a particular storm. If for a given input channel we call the times of entry t_i (where $t_i < t_{i+1}$) and the corresponding data points v_i, the computer built a time function v(t) which gave an interpolated value of v at any time t. For an interpolation algorithm, the computer used a simple step-function fit to the tabulated data points, making $v(t) = v(t_j)$ when $t_j \leq t \leq t_{j+1}$.

After each time function was generated, the computer numerically averaged it over a 15-second window to generate the average signal and rain rate values required for comparison with the steady-state theoretical calculations. Since about 15 data points contributed to each 15-second average value of each signal, the errors introduced into the average by the step-function time interpolation were minor.

The signal averaging was done by linearly averaging dB values to get a dB average. The alternative would have been to convert signal values from dB to watts, average these to get the average signal level in watts, and convert this figure to an average signal level in dB. The two methods should usually give the same or very nearly the same results; in cases of difference, it was felt that the dB average more nearly filled the needs of the communications system designer.

The path average rainfall rate for any time was computed by averaging the interpolated rain rate from each reporting gauge at that time. The computer then time-averaged the path average rainfall rate over a 15-second window to generate an "average rain rate" parameter for use in the data display.

4.2.2. Display

For most storms, eleven graphs were generated. These were:

1. Path-average rainfall rate versus time,
2. Cross polarization isolation versus time,
3. Attenuation versus time,
4. Cross polarization isolation versus rain rate scatter plot,
5. Average cross polarization isolation for each channel versus rain rate,
6. Average cross polarization isolation versus rain rate (channels combined),
7. Attenuation versus rain rate scatter plot,
8. Average attenuation for each channel versus rain rate,
9. Average attenuation versus rain rate (channels combined),
10. Attenuation versus cross polarization isolation scatter plot, and
11. Average attenuation versus average cross polarization isolation (channels combined).

All of the available graphs for each storm studied during this project appear in Interim Report II. This chapter will emphasize the highlights of the data and summarize the observed agreement between theory and experiment.

4.3 Factors Influencing the Experimental Data Which The Theory Disregards

4.3.1 Introduction

The theory of rain depolarization developed in Chapter 2 and expanded in Chapter 3 to include an entire communications system is essentially a steady-state theory. At a given rain rate it predicts the mean cross polarization isolation that will be observed and the limits between which the isolation at that rain rate will lie. When cross polarization is measured experimentally, consistent agreement with theory requires that

(a) a sufficient number of points be taken to generate a meaningful average value of isolation at each rain rate of interest, and

(b) experimental conditions closely approximate the assumptions of the theoretical model.

Insofar as thes requirements depend on cooperation by the rain, they are beyond the control of the experimenter. The experimental data must be evaluated with (a) and (b) in mind so that valid points which should be compared with the theory can be separated from measurements that were made under questionable conditions. The following sections explore several factors which bear on the experimental results and which should be explored before theory and experiment are compared.

4.3.2 The Effect of Rain Inhomogeneity Along the Propagation Path*

4.3.2.1 Introduction. Existing theoretical models for millimeter wave rain depolarization assume a rain rate distribution that is uniform

---

*This section was contributed by Capt. James L. Hogler, U. S. Army.

along the propagation path and the comparisons between theory and experiment that will be made in this report are based on a calculated path average rain rate. However, the nature of a real storm is such that the rainfall measured at discrete points along the path is not uniform and the question as to the validity of using a path average rain rate for reliable predictions must be answered. Logically, one can justify this assumption for short paths and fairly uniform storms, but the logic is questionable for long paths or for high intensity rain rate variations over short paths. This section discusses depolarization predictions for a path with a variable rain rate and explores the errors introduced by prediction of uniform rain rate along the path.

4.3.2.2 Model Development. The scattering model was modified to accept five discrete, but different rain rates along a given propagation path. The selection of five subpaths was made to conform with the use of five uniformly-spaced rain gauges in this project. Each of the five subpaths were of equal length (one-fifth of the total propagation path). Rain rates were assumed to be uniform along each subpath. The model then calculated the cross polarization level along the entire path using the depolarization introduced by each subpath rain rates.

4.3.2.3 Theoretical Analysis. The scattering model uses the drop population of the first Fresnel zone to predict rain depolarization, and when subpaths are treated the integrity of the first Fresnel zone must be maintained. This means that the depolarizing effect of the entire path is different from the depolarization that would be calcu-

lated from simply taking the five subpaths in series because the subpath Fresnel zones are smaller than the total path Fresnel zone and the drop population is reduced accordingly. The loss of total path Fresnel zone integrity would change the entire problem.

Fresnel zone integrity can be maintained in the scattering model for variable rain rate by calling on the translocation theorem. This states that the effects of the scattering drop planes are independent of position along the path. The translocation theorem combined with the numerical summation process used in the scattering model allows one to use subpaths of various rain rates and still maintain the total Fresnel zone integrity. First, establish the rain rate for each of the five subpaths. Then, using the polarization of the transmitted wave as the polarization incident on the first subpath, calculate the output polarization from the first subpath. This is easily done for the first subpath by using the total path Fresnel zone but only letting the summation of path segments run from 1 to N/5 rather than 1 to N (as would be the case if the rain rate were uniform over the total path). Making use of the translocation theorem assume that subpath two is in the first subpath position. Letting the output polarization from subpath one be the incident polarization on subpath two, again calculate the output polarization by summation of segments from 1 to N/5. This process is repeated using N/5 summations for each of the remaining three subpaths.

The output polarization of the wave from the fifth segment will be the final polarization state of the wave. By summing each subpath as N/5 segments one has used a total of N segments to define the total

path Fresnel zone effects, and the total Fresnel zone volume has been maintained. The effect of using N/5 segments is the same as calculating the depolarization effects for a given rain rate over 1/5 of the total path which is what the model must do if it is to be used to analyze rain variation along the path.

4.3.2.4. Example Storms. To test the results under various storm conditions and path lengths, three path lengths and seven example storms were used. The three path lengths used were 1,000, 5,000 and 10,000 meters. All calculations were made at 19.3 GHz; this parameter can also be changed in the model by inclusion of the proper scattering coefficients.

Seven storm combinations were used for various data comparisons. The storms (displayed in Figure 4-1) are as follows:

1 and 2 Storm 2 is the inverse of storm 1. This means that the first segment rain rate of storm 2 is the fifth segment rain rate of storm 1. This inversion is followed for the entire storm. The purpose of this storm pair is to see the effects of depolarization on a full duplex system where transmitters and receivers are located at both ends of the path and operating in both directions simultaneously. Both transmitters see the same mean storm; however, the order of the various subpaths are reversed.

3 This storm represents a radically changing storm where there is not uniform variation along the path. This storm is best described as a series of step functions.

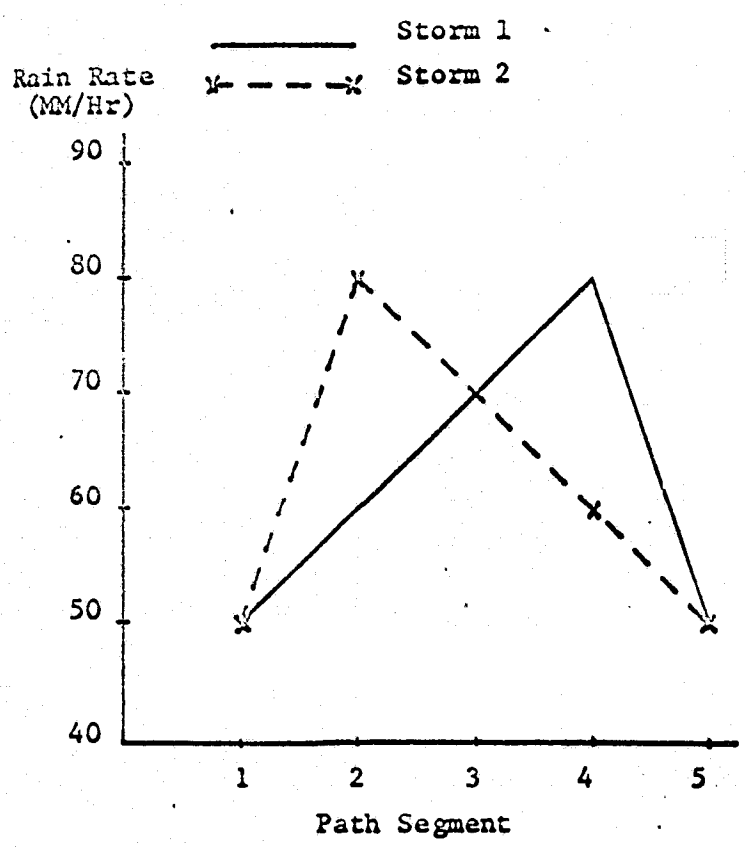

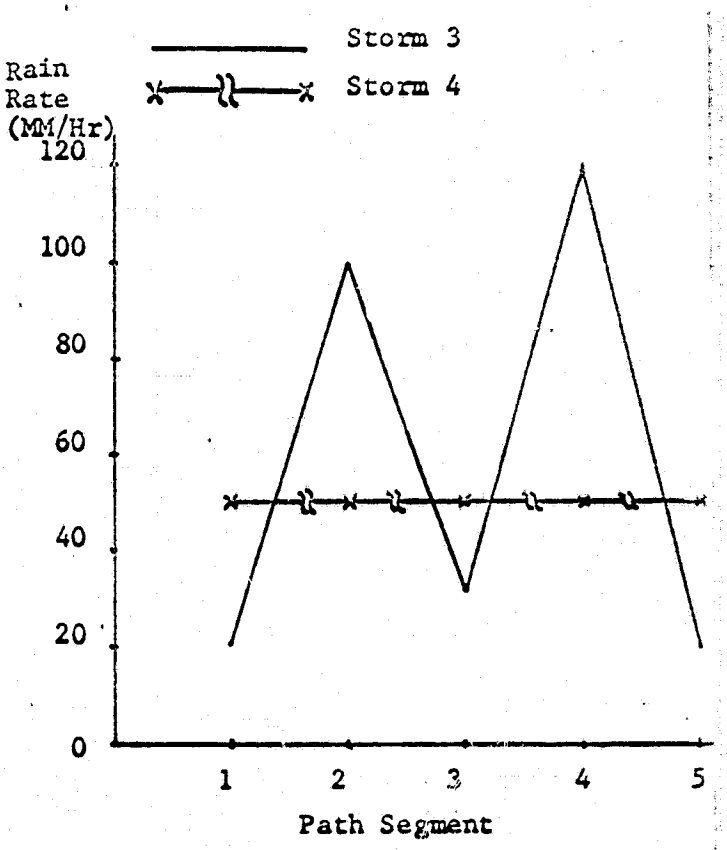

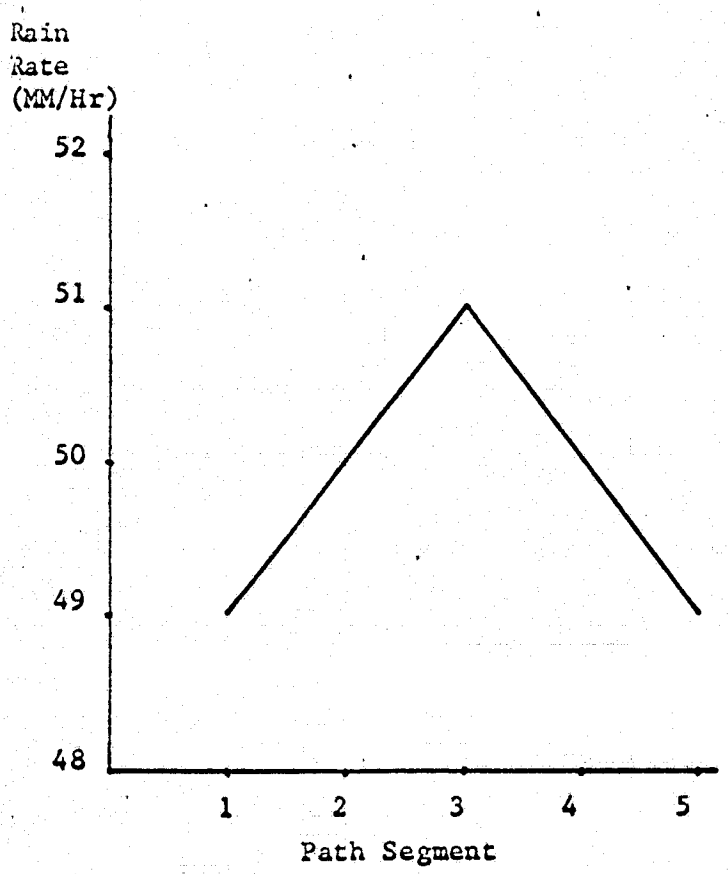

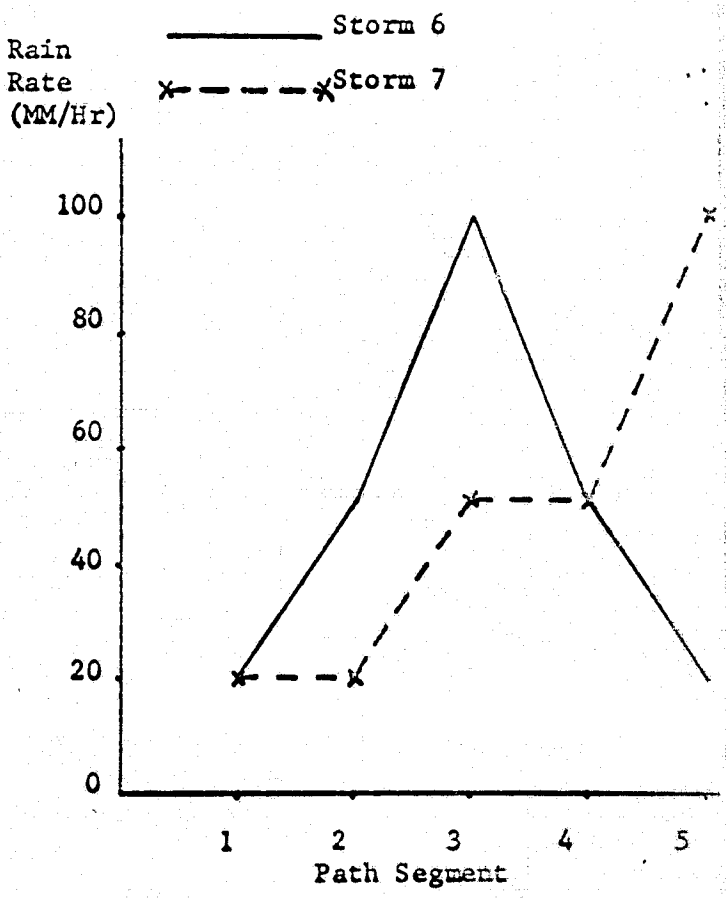

Figure 4-1: Simulated Storms Used to Investigate the Effects of Rain Inhomogeneity

The variation is so pronounced that the standard deviation of the entire storm is almost equal to the average rain rate.

4 This storm is a completely uniform storm with identical rain rates on each subpath. This storm was included to serve as a validity check on the model.

5 Storm 5 represents a storm which is fairly uniform along the path. As contrasted with storm 3 the standard deviation of the storm is less than 1 mm/hr for the path.

6 and 7 These storm combinations were chosen to investigate storm composition along a path. Both storms have the same five rain rates for subpaths; however, the values are "normally" distributed for storm 6 and monotonically increasing for storm 7.

For all storms (see Table 4-1) the path average and exact cross polarization levels agree to within 0.2 dB. The greatest difference for all path lengths considered occurs in storm 3. This is to be expected since storm 3 varies the most along the path; however, even in this case the difference is almost negligible for engineering purposes. The difference is truly negligible for the gradually changing storm 5. Since it is highly unlikely that an actual storm would vary more radically than storm 3, particularly when the total path length is only 1,000 meters, one can conclude that path average calculations are valid for engineering design purposes within those ranges included herein and that rain rate inhomogeneity introduces negligible error into the data recorded for this project.

Table 4-1 The Effect of Rain Inhomogeneity on Calculated Cross Polarization Levels

Storm No.	Path Avg.* XPOL (dB)	Segments* XPOL (dB)	Diff* (dB)	Path Avg.† XPOL (dB)	Segments† XPOL (dB)	Diff† (dB)	Path Avg.** XPOL (dB)	Segments** XPOL (dB)	Diff** (dB)
1	-26.03067	-26.02188	.00879	-11.95938	-11.95032	.00906	-5.73274	-5.72520	.00754
2	-26.03067	-26.02188	.00879	-11.95938	-11.950.36	.00902	-5.73274	-5.72499	.00775
3	-26.73012	-26.92769	.19757	-12.66815	-12.42371	.24444	-6.45992	-6.24045	.21947
4	-28.31012	-28.31012	0	-14.26530	-14.26530	0	08.09755	-8.09755	0
5	-28.35326	-28.35315	.00011	-14.30878	-14.30878	.00005	-8.14209	-8.14200	.00009
6	-28.75044	-28.53806	.21238	-14.70941	-14.49336	.21605	-8.55208	-8.34341	.20867
7	-28.75044	-28.53813	.21231	-14.70941	-14.49278	.21663	-8.55208	-8.34444	.20764

* Path Length = 1,000 meters, Path Segments = 500, Subpath Length = 200 meters, Subpath Segments = 100.

† Path Length = 5,000 meters, Path Segments = 1,000, Subpath Length = 1,000 meters, Subpath Segments = 200.

** Path Length = 10,000 meters, Path Segments = 2,000, Subpath Length = 2,000 meters, Subpath Segments = 400.

4.3.3 The Effect of Drop Size Fluctuations

The scattering model assumes implicitly that the waves interact only with drops of the Laws and Parsons [1943] modal size. Since a real rain contains a wide distribution of drop sizes, a significant amount of millimeter wave interaction with non-modal drops will occur. This will produce a distribution of cross polarization levels around the modal-scattering mean; and it is an effect that the steady-state scattering model does not include.

An extensive investigation of this problem by J. L. Hogler [1974] concludes that for a 1000 m path at 19.3 GHz fluctuations in the drop population would produce a cross polarization isolation distribution with a standard deviation of 3 dB about the predicted mean. The 3 dB figure should be a good approximation for the 1430 meter 17.65 GHz path used in this report.

4.3.4 Averaging Time

Early in this project a 15-second averaging time was adopted as standard for all data. Data for a representation storm (17 August 1972) were compared for averaging times of .01, 1, 5, 10, and 20 seconds and no significant differences were detected so far as average isolations and attenuations for each integer rain rate value are concerned. This indicates that time-averaging effects are eliminated (as they should be) when the ensemble of points corresponding to each integer rain rate is averaged.

4.3.5 Conclusions

None of the effects discussed in this section should cause significant deviations between our average experimental data and the

theoretical predictions. Drop size fluctuations should introduce some statistical scatter into the isolation data; this effect will be included when the data are evaluated.

4.4 Cross Polarization Isolation

4.4.1 Expected Behavior of the Data

4.4.1.1 Statistical Effects. If the theory developed in this report is correct and our experimental conditions matched our theoretical assumptions, within each storm, the average cross polarization isolations measured for each channel at a given rainfall rate should equal those calculated from equations (3-83) and (3-84). To the extent that the system clear-weather isolations remain constant, equations (3-76) and (3-77) should also equal the measured isolations for the entire project. Any single data point (i.e. any one 15-second running average cross polarization isolation) should fall between the upper and lower limits set by equations (3-78) through (3-81), plus or minus some additional factor to account for interactions with drops larger or smaller than the mode. It is difficult to predict the expected scatter between successive data points measured at the same rain rate, but a tentative estimate of the standard deviation of the isolation distribution at each rain rate can be made.

First consider the effect of phase fluctuations along the path. These influence the last terms of equations (3-76) and (3-77); each term represents the mean-square value of a Rayleigh phasor [Beckmann, 1967]. If the first term in these equations is constant and all drops are of the modal size, then the scatter in the measured isolation values

would result solely from scatter in the last term. The standard deviation of the amplitude of a Rayleigh phasor is 0.46325 times the RMS value; signals (voltage levels) one standard deviation above the RMS value are at 1.46325 times the RMS value or 3.31 dB above it. Hence, our experimental data should show a standard deviation of 3.31 dB (independent of rain rate) due to phase fluctuations.

If the phase fluctuations are suppressed, Hogler's [1974] work indicates that we should see a 3 dB standard deviation in the isolation data becuase of statistical variations in the drop size. The drop size and phase effects are statistically independent so that the total variance of the cross polarization isolation is equal to the sum of the variance due to drop size fluctuations and the variance due to phase fluctuations. If the RMS isolation expressed as a numerical ratio of E fields (rather than in dB) is I_o, then a 3 dB standard deviation due to drop-size effects relative to I_o corresponds to a numerical standard deviation of 1.4125 I_o and a variance of 1.9953 I_o^2. Similarly, a 3.31 dB standard deviation relative to I_o due to phase fluctuations corresponds to a numerical standard deviation of 1.4639 I_o and a variance of 2.1429 I_o^2. The combined variance is 3.6068 I_o^2 and the combined standard deviation is then 1.8992 I_o or 5.57 dB. This means that if the theory is completely correct, the average measured isolation at each rain rate should coincide with the theoretical value (if a sufficiently large number of points contribute to the average) and the distribution of points around the average should have a standard deviation of about 5.6 dB.

4.4.1.2 Canting Angle Effects. Because information on the statistical properties of the raindrop canting angle is lacking, canting angle effects were not included in the discussion above. This omission is justified by our theoretical results, which indicate that canting angle has a very minimal effect for our path, 17.65 GHz operating frequency, and $\pm 45^{\circ}$ linear polarization. Table 4-2 displays theoretical values of path cross polarization isolation (antenna effects are neglected) as a function of rain rate for canting angles of 0 and $\pm 5^{\circ}$. The maximum effect of a 5° change in canting angle is about 0.6 dB. [This table and those which follow are calculated at 19.3 GHz; this is the closest frequency to 17.65 GHz for which scattering coefficients are available.]

4.4.1.3 The Percentage of Oblate Drops. The percentage of oblate drops has a strong influence upon the path cross polarization isolation and it is perhaps the one factor about which there is the least agreement among researchers. Our English colleagues use 100%; in this project we have adopted a 40% figure based on Jones' [1959] work; [See Interim Report I] Table 4-2 and the theoretical curves in Interim Report II are calculated for the 40% figure. Table 4-3 presents calculated isolation values for path and polarization with 40% and 100% oblate drops. Note that with 100% oblate drops there is about 7.87 dB less isolation at a given rain rate than there is with 40% oblate drops.

4.4.2 Comparing Theory and Experiment

A study of the data presented in Interim Report II indicates that the theoretical model developed in this project agrees well

Table 4-2 Path Isolation as a Function of Rain Rate and Canting Angle for $\pm 45^{o}$ Linearly Polarized 19.3 Signals Propagating Over a 1.43 Km Path

Rain Rate (mm/hr)	Isolation in dB		
	$\Theta = -5^{o}$	$\Theta = 0^{o}$	$\Theta = +5^{o}$
10	-42.939	-42.801	-42.929
30	-31.668	-31.512	-31.622
50	-25.768	-25.558	-25.614
70	-21.960	-21.681	-21.670
90	-19.214	-18.859	-18.772
110	-17.093	-16.658	-16.492
130	-15.738	-14.861	-14.614
150	-13.947	-13.346	-13.017

Table 4-3 Path Isolation as a Function of Rain Rate and % of Oblate Drops for $\pm 45^{o}$ Linearly Polarized 19.3 GHz Signals Propagating Over a 1.43 Km Path

Rain Rate (mm/hr)	Isolation in dB		
	40% Oblate	100% Oblate	Difference
10	-42.801	-34.843	7.958
30	-31.512	-23.563	7.949
50	-25.558	-17.629	7.929
70	-21.681	-13.781	7.900
90	-18.859	-10.995	7.864
110	-16.658	- 8.839	7.819
130	-14.861	- 7.098	7.763
150	-13.346	- 5.653	7.783

with the data. The plotted experimental points are in close proximity to the theoretical values of path isolation - particularly at high rain rates where antenna effects are the least significant. The agreement at low rain rates may be improved by including the antenna properties as in the curves of Figure 3-1. When the channels are considered separately, the standard deviations of the measured isolations at each rain rate almost never exceed the expected 5.57 dB. So far as the theoretical model is concerned, we conclude that it has been verified subject to the experimental considerations advanced in the previous sections. There is a small tendency for our measured values to indicate slightly less isolation at a given rain rate than the theory indicates. Since this effect is almost independent of rain rate, the most probable explanation is that our 40% oblate drop estimate is slightly low. To be conservative, a communication system designer might want to use 50% or 60% oblate drops to allow a safety margin.

Wind should affect rain depolarization primarily through the canting angle, and, hence, the effect of wind on depolarization should be minor. Our data comfirm this; we found no correlation between wind and isolation measurements.

Perhaps the most intriguing feature of the data is the nearly constant separation between I_{-+} and I_{+-}. If at each integer rain rate one compares the average measured I_{-+} and the average measured I_{+-} for the entire project, the average difference is 3.797 dB. This effect is almost certainly a result of the antennas, but it is more complex then the assumptions that lead to Figure 3-1 would allow,

since Figure 3-1 shows all isolation curves joining at sufficiently high rain rates.

Obviously, neither the transmitting antenna nor the receiving antenna is ideal, and it is possible that this constant decibel separation between I_{-+} and I_{+-} can be explained if the receiving antenna terms are retained in the development leading to equations (3-76) through (3-84). In deriving these equations, we explicitly assumed a non-ideal transmitting antenna and an ideal receiving antenna. The problem should be explored further without this assumption.

Indeed, after several years of effort in the field, it is the authors' opinion that the present understanding of the depolarizing effects of rain is now somewhat ahead of the current understanding of the polarization properties of antennas. For a given antenna, all of the data necessary to use the theory developed in Chapter 3 are simply not available, and we recommend further research on accurately predicting the response of real dual-polarized antennas to waves of arbitrary polarization.

4.5 Attenuation

4.5.1 Introduction

The primary goal of this project was to measure the depolarizing effects of rain. A necessary byproduct of the depolarization measurements was the collection of an equal amount of attenuation data, and a secondary mission was to investigate the dependence of attenuation on rain rate and on the transmitted polarization.

4.5.2 General Discussion

Attenuation is both easier and harder to measure than cross polarization isolation. It is easier because it is so much less sensitive to antenna effects; nothing like the complicated development of Chapter 3 is necessary to explain the dependence of attenuation data on antenna characteristics. Rain attenuation is measured with respect to a clear weather reference signal, and the antenna gain together with the transmitter power and receiver gain determine this reference signal. But this simplicity also contributes to the difficulty: for rain attenuation to be measured the clear weather reference signal must be known, and for attenuation values from one storm to be compared with attenuation values from another, both should have had the same reference signal.

The problem is that the clear weather reference signal changes with time as the transmitter power and receiver local oscillator frequency drift. (This reduces the receiver gain.) These drifts have no effect on depolarization data, because the copolarized and cross polarized signal levels are affected in exactly the same way, but they throw attenuation measurement off if the clear weather reference signal is not checked before each storm begins.

At the start of each storm our system averaged the received signals on each channel for 30 seconds and used these values as clear weather reference signals. This procedure worked well for storms which started slowly; in cases where the onset of intense rain was rapid it led to negative attenuation at low rain rates. For each storm and each channel, this was corrected (if necessary) by adding a constant to each attenuation value such that all values were positive or zero.

The effect of this process is that, for a given storm, the attenuation values for each channel may all be off by the same small amount (1 or 2 dB). The attenuation for the two channels may also differ by a constant number of dB. The theoretical and measured attenuation values for each channel should lie along parallel lines; these lines will be offset by an amount (in dB) equal to the difference between their assumed clear weather reference signals.

In contrast to the apparent changes in attenuation caused by incorrect clear weather reference signals, the effects of canting angle and percentage of oblate drops are negligible. This is evident from Tables 4-4 and 4-5.

4.5.3 Comparing Theory and Experiment

The data presented in Interim Report II generally show good agreement between theoretical and measured values of rain attenuation. Following the pattern noted by de Bettencourt [1973] and others, measured values tend to be slightly above the theoretical at the lower rain rates.

At very high rain rates (90 mm/hr and above) we have observed somewhat surprising results. Usually measured attenuations in this range fall significantly below the theoretical predictions. Norbury and White [1973] have made a convincing argument that this results from erroneous rain gauge data; their feeling is that at high rain rates conventional rain gauges simply cannot keep up with the rain. Some of our data contradicts this conclusion, since in our most intense storm [that of May 28, 1973; see Interim Report II] measured and

Table 4-4 Attenuation as a Function of Rain Rate and Canting Angle for $\pm 45^{\circ}$ Linearly Polarized 19.3 GHz Signals Propagating over a 1.43 Km Path.

Rain Rate (mm/hr)	Attenuation in dB $\Theta = -5^{\circ}$	$\Theta = 0^{\circ}$	$\Theta = +5^{\circ}$
10	1.349	1.354	1.358
30	4.162	4.185	4.207
50	6.964	7.041	7.118
70	9.768	9.912	10.058
90	12.573	12.793	13.014
110	15.378	15.678	15.979
130	18.183	18.564	18.948
150	20.987	21.451	21.917

Table 4-5 Attenuation as a Function of Rain Rate and % of Oblate Drops for $\pm 45^{\circ}$ Linearly Polarized 19.3 GHz Signals Propagating over a 1.43 Km Path

Rain Rate (mm/hr)	Attenuation in dB 40% Oblate	100% Oblate	Difference
10	1.354	1.352	0.002
30	4.185	4.171	0.014
50	7.041	6.997	0.044
70	9.912	9.827	0.085
90	12.793	12.654	0.139
110	15.678	15.475	0.203
130	18.564	18.284	0.280
150	21.451	21.076	0.375

theoretical attenuation values were in excellent agreement for all 15-second average rain rates between 10 and 138 mm/hr. On the other hand, our other two most intense storms [August 17, 1972, and March 16,1973] showed measured attenuations below the theoretical values at very high rain rates. Perhaps Mink [1973] is correct in his conclusion that at some rainfall rates the drop size distribution varies considerably from storm to storm.

4.6 Isolation Versus Fade

If measured attenuation is plotted versus measured isolation with time or rain rate as a parameter, the resulting curve should be relatively insensitive to errors in measuring the rain rate. P. A. Watson brought the authors' attention to these "isolation versus fade" curves and a large set of them appears in Interim Report II. Their characteristic shape is determined by the relationship between attenuation and isolation; errors in attenuation measurement due to an incorrect clear weather reference signal will shift a measured curve up or down without changing its shape. In Interim Report II our measured data are compared to theoretical isolation versus fade curves calculated for 19.3 GHz which do not include antenna effects. Nevertheless, the agreement between theory and experiment is well within the limits of accuracy with which the attenuation measurements were made.

4.7 A Note on Phase

Ther is some interest in the way in which the phase of a received signal depends on polarization and rain rate and during this project an unofficial attempt at studying phase effects was made. The relative phase difference between the two receiver channels was measured during several storms in 1973 and, to the limited accuracy of the available equipment, this differential phase remained constant during each storm. This result supports the theoretical conclusion that the differential phase difference between coherent $+45^{\circ}$ and -45° linearly polarized signals is insensitive to rain rate and canting angle.

4.8 A Note on Snow Depolarization

Little quantitative information on the depolarizing effects of snow is avilable. A theoretical analysis of the problem is not yet possible because data on the scattering properties of snowflakes and on their shape and size distribution do not exist. Experimental measurments require a location where snow is frequent and instruments to measure snowfall rate and water content accurately and to date no one has conducted an experiment devoted primarily to snow depolariaation.

At NASA's request we modified our equipment to measure snow depolarization and waited for snow storms from January 1 through March 31, 1974. We observed one storm which began on January 19 at about 10:00 AM and ended at about 1:00 PM after depositing 100mm of snow. During the storm cross polarized and co-polarized signal components were recorded and the snowfall rate was computed from

measurements of the snow depth at a convenient point on the ground. The results of our measurement are displayed in Figure 4-2.

Snow had no effect on the channel with the poorer residual isolation, but the isolation for the other channel behaved unexpectedly, showing better isolation during the storm than it did before or after. This change in isolation was not accompanied by any noticeable attenuation effects; indeed the snow attenuation was almost negligible for the entire storm.

The reason that snow had this effect on cross polarization isolation remains unknown. With measurements on only one storm many hypotheses are possible. The authors hope that further measurements of the depolarizing effects of snow will be made in the future.

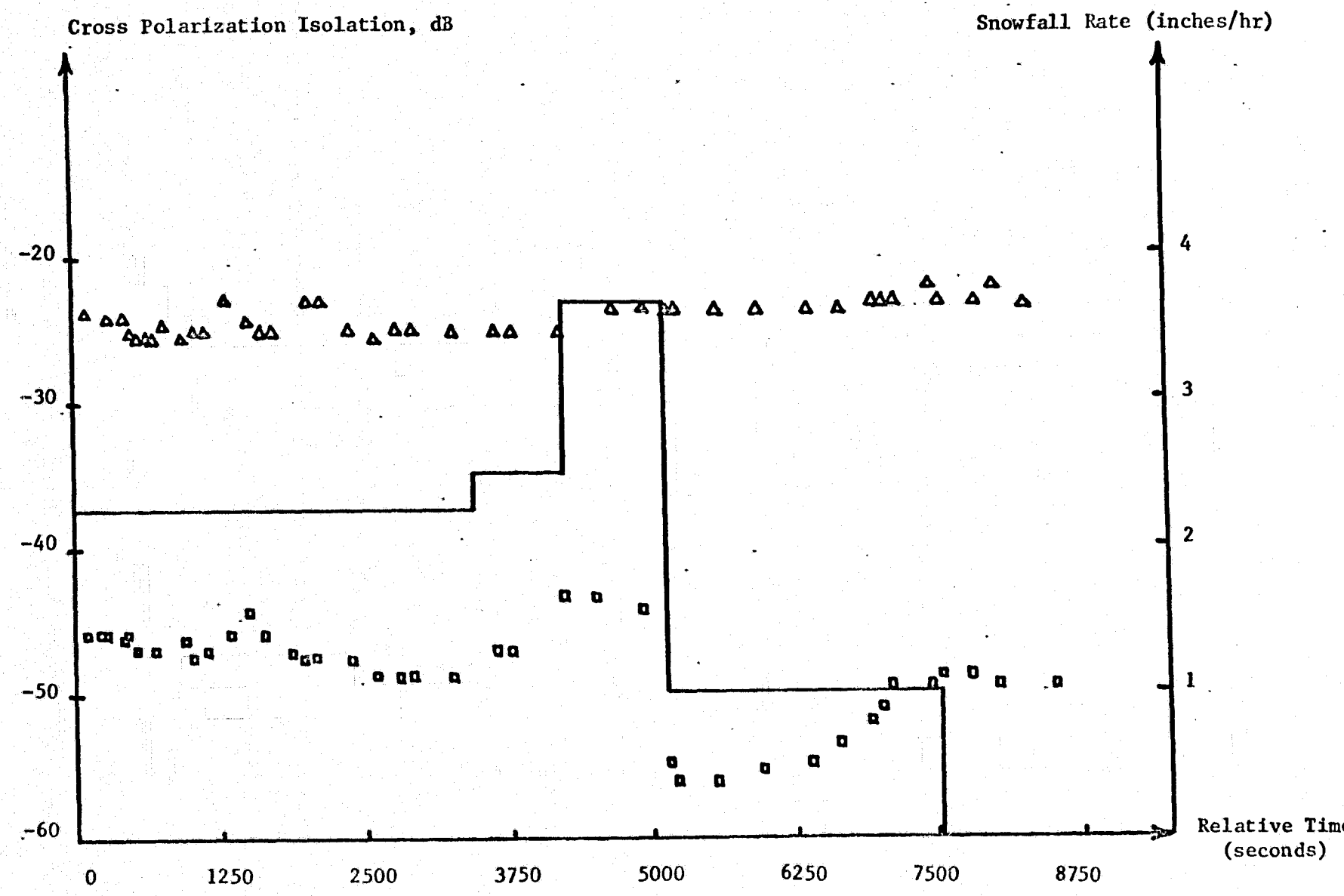

Figure 4-2: Snow Depolarization Data for January 19, 1974

5. Conclusion

This project began with questions about rain depolarization and the effects of polarization on rain attenuation in millimeter wave radio systems. In this report we have presented a theoretical model for rain effects that agrees well with our experimental data and which predicts the likely interference levels in terrestrial polarization diversity and frequency - sharing applications. Subsequent research will extend the methods described here to earth-satellite paths.

6. Literature Cited

1. P. Beckmann, Probability in Comunications Engineering. New York: Harcourt, Brace,and World, Inc., 1967, pp. 118-120.

2. A. C. Best, "Empirical Formulae for the Terminal Velocity of Water Drops Falling Through the Atmosphere," Quart. J. R. Met. Soc., Vol. 76, pp. 302-311, July 1950.

3. J. T. deBettencourt, "Statistics of Terrestrial Millimeter-Wave Rainfall Attenuation", presented at IUCRM colloquium on the Fine Scale Structure of Precipitation and EM Propagation, Nice, France, October 1973.

4. D. C. Hogg, "Depolarization of Microwaves in Transmission through Rain," in Telecommunications Aspects on Frequencies Between 10 and 100 6Hz, NATO/AGARD Conference Proudings No. 107, April 1973. (Available through NTIS)

5. J. L. Hogler, "Rain Depolarization Scatter Prediction," M.S. Thesis, Virginia Polytechnic Institute and State University, Blacksburg, Virginia, 1974.

6. D. M. A. Jones, "The Shape of Raindrops," Journal of Meteorology, Vol. 16, pp. 504-510, October 1959.

7. J. D. Kraus and K. R. Carver, Electromagnetics (Second Edition). New York: McGraw - Hill, 1973, pp. 435-441.

8. J. O. Laws and D. A. Parsons, "The Relation of Raindrop-size to Intensity," Trans. Am. Geophysical Union, Vol. 24, pp. 432-460, 1943.

9. J. W. Mink, "Rain Attenuation Measurements of Millimetre Waves Over Short Paths," Electronics Letters, Vol. 9, pp. 198-199, May 1973.

10. J. R. Norbury and W. J. K. White, "Correlation Between Measurements of Rainfall Rate and Microwave Attenuation at 36 6Hz," in Propagation of Radio Waves at Frequencies Above 10 6Hz (IEE Conference Publication Number 98). London: IEE, 1973, pp. 45-51.

11. T. Oguchi, "Attenuation and Phase Rotation of Radio Waves Due to Rain: Calculations at 19.3 and 34.8 6Hz," Radio Science, Vol.8, January 1973.

12. D. T. Thomas, "Cross Polarization Distortion in Microwave Radio Transmission Due to Rain," Radio Science, Vol. 6, No. 10, pp. 833-840, October 1971.

13. H. C. van de Hulst, Light Scattering by Small Particles. New York: John Wiley Sons Inc., 1957.

14. P. A. Watson, "Crosspolarization Isolation and Discrimination," Electronics Letters, Vol. 9, pp. 516-517, November 1973.

15. P. Watson and M. Arbabi, "Rainfall Cross Polarization at Microwave Frequencies," Proc. IEE (London), Vol. 120, pp. 413-418, April 1973.

16. P. H. Wiley, W. L. Stutzman, and C. W. Bostian, "A New Model For Rain Depolarization," Paper I. 10, International Union Committee on Radio Meteriology Colloquium on the Fine Scale Structure of Precipitation and Electromagnetic Propagation, Nice, France, 1973. (This paper will appear in Journal de Recherches Atmospheriques in 1974).